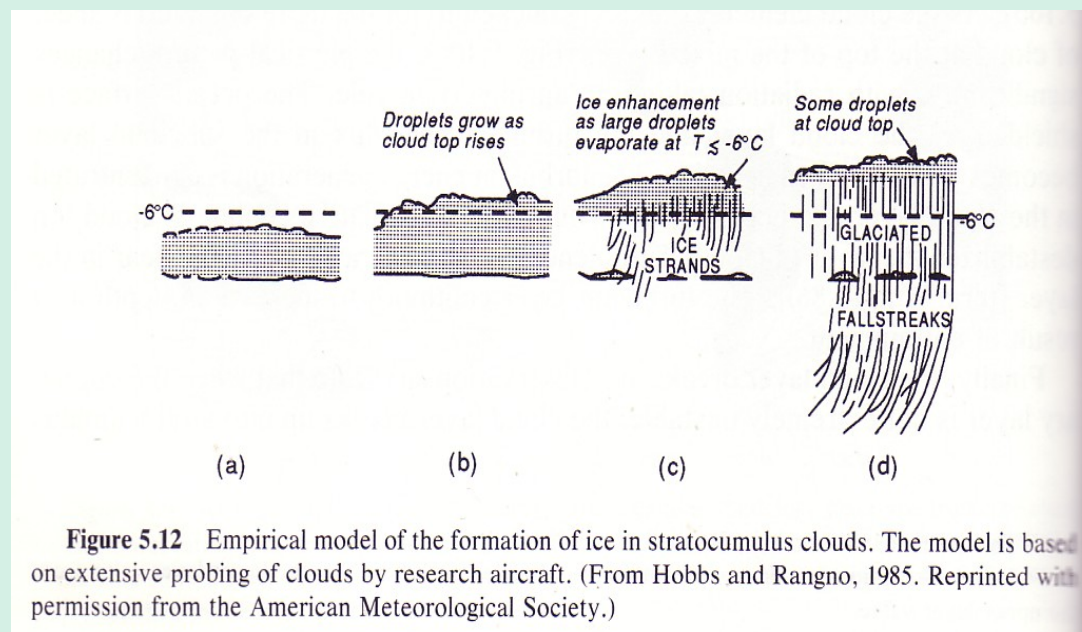# Ch. 6 Cloud/precipitation Formation and Process:

- Reading: Text, ch. 6.1-6.6, p209-245
- Reference: Ch.3 of "Cloud Dynamics" by Houze
- Topics:
  - Cloud microphysics: cloud droplet nucleation and growth, precipitation process
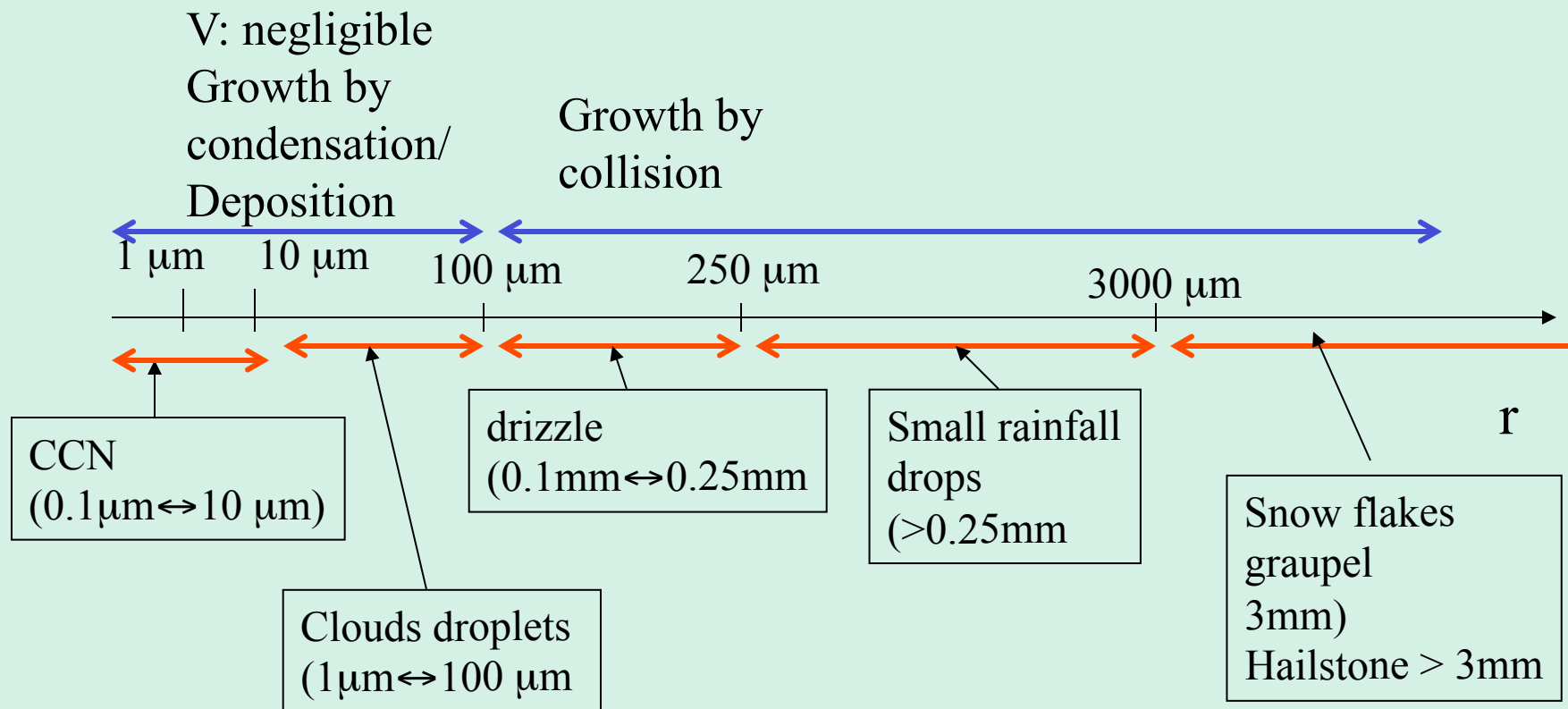 - Cloud dynamics: the dynamic conditions determine the formation and development of clouds

Cloud/Precipitation Microphysics:

- What control the growth-dissipation of cloud droplets and falling of precipitation drops?
- Cloud microphysics also determine the precipitation efficiency

Figure 5.12 Empirical model of the formation of ice in stratocumulus clouds. The model is based on extensive probing of clouds by research aircraft. (From Hobbs and Rangno, 1985. Reprinted with permission from the American Meteorological Society.)

Size determines falling speed, cloud or precipitation

- Define CCN, Cloud, drizzle and precipitation droplets

V: negligible
Growth by
condensation/
Deposition

Growth by
collision

1 μm   10 μm   100 μm   250 μm   3000 μm

r

CCN
(0.1μm↔10 μm)

Clouds droplets
(1μm↔100 μm

drizzle
(0.1mm↔0.25mm

Small rainfall
drops
(>0.25mm

Snow flakes
graupel
3mm)
Hailstone > 3mm

Growth of warm (liquid) clouds

- When r < 0.1 mm, fall speed is negligible, cloud droplets grow from condensation
- When r > 0.1 mm, fall speed increases and collision between cloud droplets (coalescence) dominates the growth.
- When r>3.5mm, breakup of drops occur

Growth by condensation

- ***Nucleation of cloud droplet:***

$$\Delta E = 4\pi R^2 \sigma_{vl} - \frac{4}{3}\pi R^3 n_l(\mu_v - \mu_l)$$

surface tension

work required to form a surface

energy change from vapor to liquid

vapor to liquid, supplies energy to form a surface

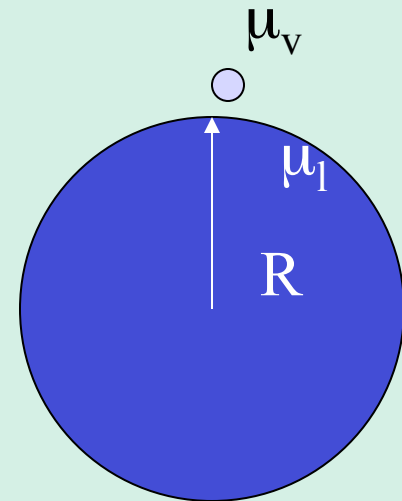ΔE : the net increase in the energy of the system due to the formation of the droplet.

R : radius of the droplet, $4\pi R^2$: *surface* area, $\frac{4}{3}\pi R^3$: volume of liquid

σ_{vl} : *work* required to create a surface

n_l : # of water molecules per unit volume in the drop

μ_v, μ_l : *Gibbs* free energy of a vapor and a liquid molecule

For a drop to grow, ΔE<0, requires large R

μ_v

μ_l
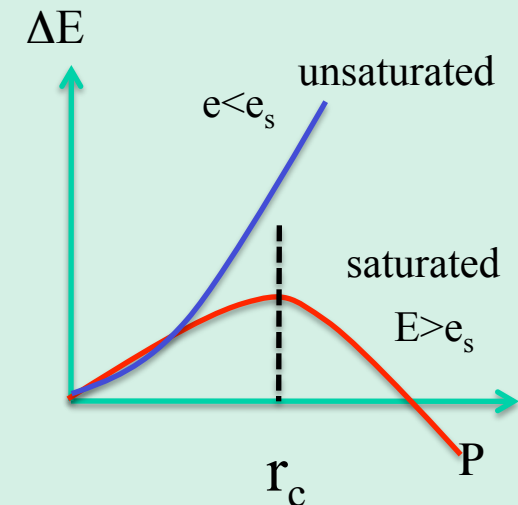
R

R>r_c (r_c: the required minimum radius, determined by $\Delta E = 0$)

$$r_c = \frac{3\sigma_{vl}}{n_l(\mu_v - \mu_l)} = \frac{3\sigma_{vl}}{n_l k_B T \ln(e/e_s)}$$

$\textit{where } \mu_v - \mu_l = k_B T \ln(e/e_s)$

$k_B : \textit{Boltzmann}$ constant

- Air must be supersaturate ($e/e_s > 1$)
- $r_c \downarrow$ with increase of supersaturation

(Graph: ΔE vs P; curves labeled "unsaturated $e<e_s$", "saturated $E>e_s$", with r_c marked on horizontal axis)

- Homogeneous nucleation: formation of a droplet from pure water vapor. This requires 300-400% supersaturation, too difficult!

- Heterogeneous nucleation: vapor condenses on a foreign object with R>R_c, such as a large aerosol particle (CCN)

- From this slide (7) to slides 13, GEO 347 is not required to master the mathematic formulas.

- Insoluble CCN: CCN only acts as a seed with R>Rc

- Soluble: e_s at wet CCN surface decreases $\Rightarrow \ln(e/e_s)\uparrow \Rightarrow R_c\downarrow$, allows nucleation on smaller CCNs. Air pollution such as SO_2 causes smoggy.

Example:

- How would the critical value ΔE* change compare to the pure water if we add sodium laurel sulfate (soap) to pure water which decreases the work for creating a surface, σ, by 10%? Note that

$$\Delta E^* = \frac{16\pi\sigma^3}{3\left(nkT \ln\frac{e}{e_s}\right)^2}$$

$$\frac{d\Delta E^*}{d\sigma} = \frac{d}{d\sigma}\left(\frac{16\pi\sigma^3}{3(nkT \cdot \ln\frac{e}{e_s})^2}\right) = \frac{16\pi \cdot 3\sigma^2}{3(nkT \cdot \ln\frac{e}{e_s})^2} = \frac{16\pi \cdot \sigma^2}{(nkT \cdot \ln\frac{e}{e_s})^2}$$

$$\frac{d\Delta E^*}{\Delta E^*} = \frac{\dfrac{16\pi \cdot \sigma^2}{(nkT \cdot \ln\frac{e}{e_s})^2} d\sigma}{\dfrac{16\pi \cdot \sigma^3}{3(nkT \cdot \ln\frac{e}{e_s})^2}} = 3\frac{d\sigma}{\sigma} = 3 \times (-10\%) = -30\%$$

- If we add sodium laurel sulfate (soap) to pure water, it would decrease ΔE* by 30%.
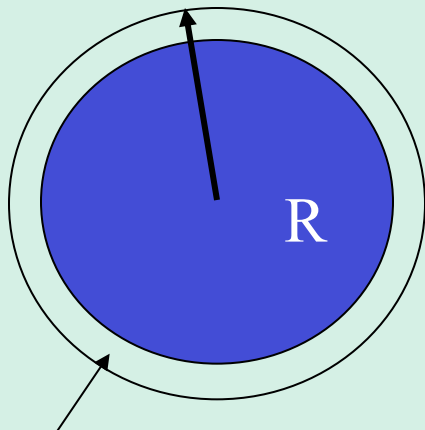
Net growth of a cloud droplet-for a plane of pure water

- *The growth of a cloud drop is determined by net flux of water molecules at the surface of a cloud droplet*

$$\frac{dm}{dt} = 4\pi R^2 D_v \frac{d\rho_v}{dr}\bigg|_R = 4\pi R D_v \left(\rho_v(\infty) - \rho_v(R)\right)$$

D_v : diffusion coefficient, mass of the droplet

$$\rho_v(r) = \rho_v(\infty) - \frac{R}{r}\left(\rho_v(\infty) - \rho_v(R)\right)$$

$\rho_v(\infty)$ **:** *ambinet* **vapor density**

For a plane of pure water :

$$\frac{dm}{dt} = \frac{4\pi R \tilde{S}}{F_k + F_C}$$

$$\tilde{S} \equiv \frac{e(\infty)}{e_s(\infty)} - 1 \text{ ambinet supersaturation}$$

$$F_K \equiv \frac{L^2}{K_a R_v T^2(\infty)} \text{ heat conductivity}$$

$$F_D \equiv \frac{R_v T(\infty)}{D_v e_s(\infty)} \text{ vapor diffusivity}$$

$D_v \dfrac{d\rho_v}{dr}\bigg|_R$ Vapor flux at the surface

κ_a: thermal conductivity
D_v: diffusivity of vapor

Net growth of a cloud droplet on a water soluble nucleus with a curved surface

$$\frac{dm}{dt} = \frac{4\pi R}{F_k + F_C}\left(\tilde{S} - \frac{\hat{a}}{R} + \frac{\hat{b}}{R^3}\right)$$

$$\frac{\hat{a}}{R} = \frac{2\sigma_{vl}}{\rho_L R_v T R} \quad \text{curvature effect}$$

$$\frac{\hat{b}}{R^3} \sim \frac{m_s M_w}{\rho_L M_s}\frac{1}{R^3} \quad \text{effect of dissolved salt on } e(R)$$

R

• *For a falling cloud droplet:*

$$\frac{dm}{dt} = \frac{4\pi R V_F}{F_k + F_C}\left(\tilde{S} - \frac{\hat{a}}{R} + \frac{\hat{b}}{R^3}\right)$$

V_F : *ventilation* factor

Growth of a cloud droplet:

- Growth of the droplet by coalescence:

$$\dot{m}_{col} = A_m \left| V(m) - V(m') \right| \rho q_{m'} \sum_c (m, m')$$

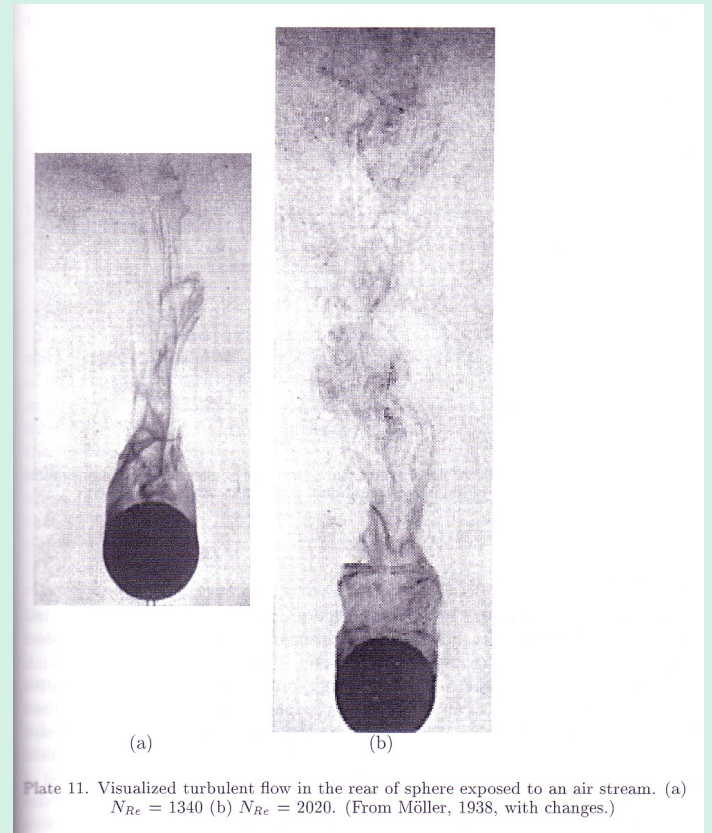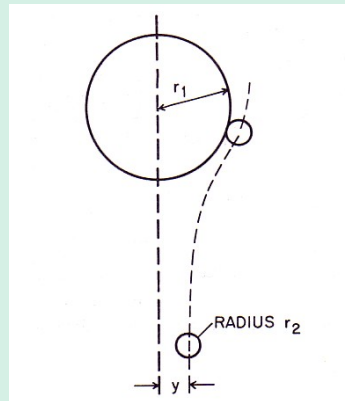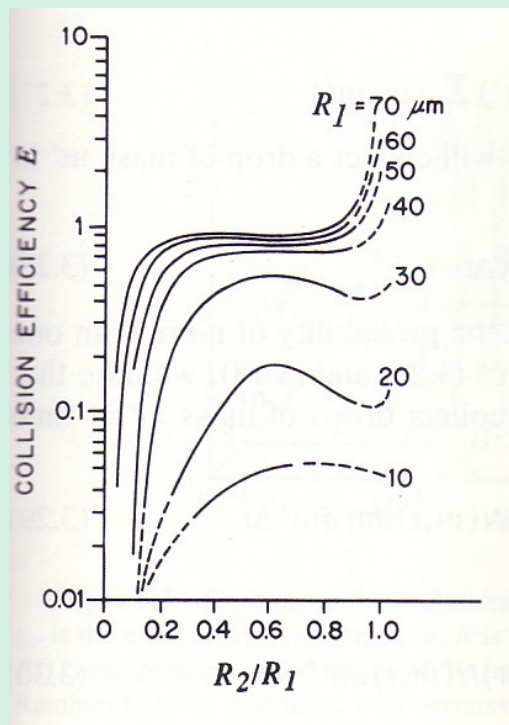$$\sum_c (m, m') \propto \frac{y^2}{(r_1 + r_2)^2} : collection \text{ efficiency}$$

$$A_m = \pi (R + R')^2 : effective \text{ cross-section area}$$

$$V : \text{ fall speed}$$

$$\rho q_{m'} : \text{liquid water content of the collected drops}$$
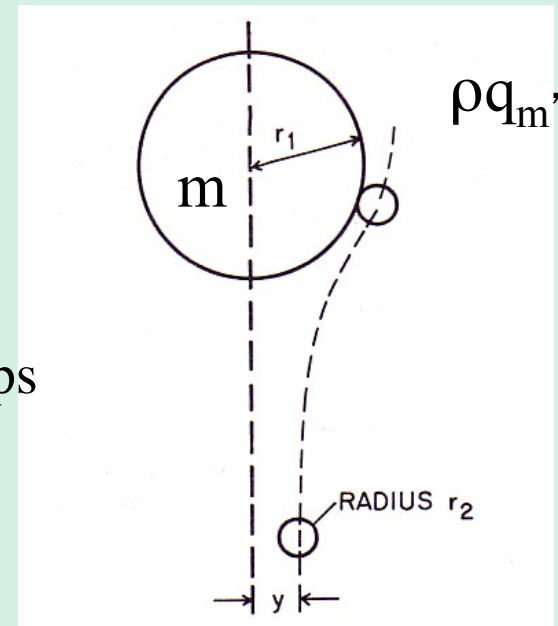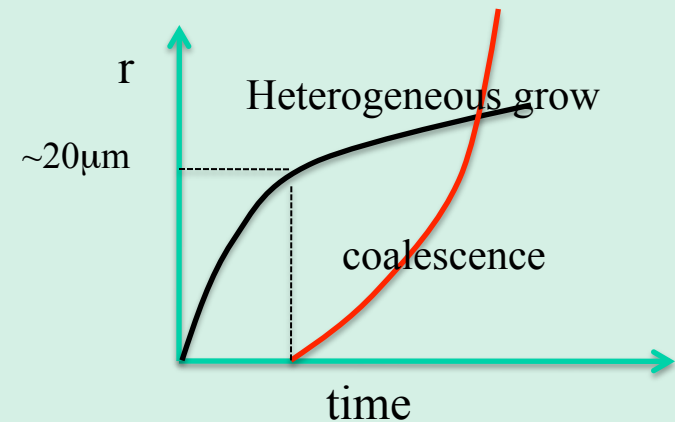
- Factors influence collection efficiency:
- Turbulence flow around the collecting drop
- Rebound problem: depends on air film trapped between the surface of two drops:
    - When two drops large enough to deform easily, the air film drainage is hindered.
    - Impact angle and relative velocity

Plate 11. Visualized turbulent flow in the rear of sphere exposed to an air stream. (a) $N_{Re} = 1340$ (b) $N_{Re} = 2020$. (From Möller, 1938, with changes.)

R_i increases with r_1, leading to eddy shedding, wake oscillation, shape deformation. The effects of these are quantified unclearly.

Fall speed

- Terminal velocity of raindrops:
  - Small droplet (<500μm): V increases nearly linearly with r
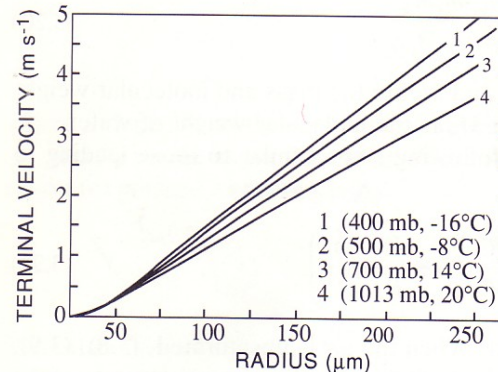 - Large droplets (mm): v increase rapidly until 3 mm, then v ➜ constant.

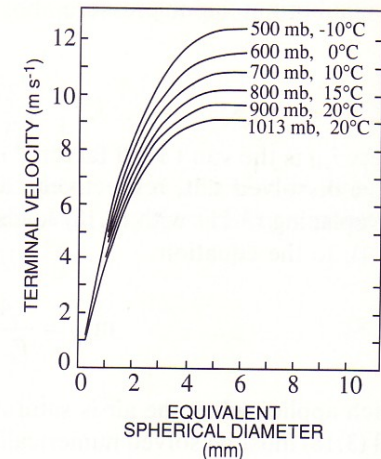$$V(r) = aD^b (\rho_{air} / \rho_l)^{1/2}$$

$$a = 2115 \ cm^{1-b} s^{-1}$$

$b = 0.8$, b = 0.5 for large drops

D : *diameter* of a raindrop

in unit of *μ*m

Figure 3.2 Fall velocity of water drops <500 *μ*m in radius for various atmospheric conditions. (From Beard and Pruppacher, 1969. Reprinted with permission from the American Meteorological Society.)

Figure 3.3 Fall velocity of water drops >500 *μ*m in radius. (From Beard, 1976. Reprinted with permission from the American Meteorological Society.)

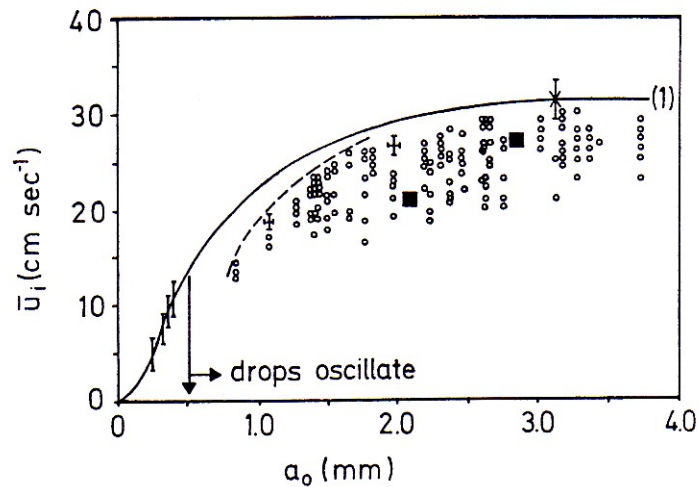# Why does V become a constant?

Fig. 10-11: Variation with drop radius of experimentally observed velocity of circulation inside water drops falling at terminal velocity in air. (I) Wind tunnel studies of Pruppacher & Beard (1970), and of Le Clair *et al.* (1972) from rotation frequency of tracer particles; (○, +) wind tunnel studies of Diehl (1989) from incomplete trajectories of tracer particles; (×) from wind tunnel studies of Schmidt (1995) from trajectories of tracer particles; (■) from wind tunnel studies of Garner and Lane (1959); line (1) based on numerical results of Le Clair *et al.*, 1972. (From Diehl, 1989, with changes.)
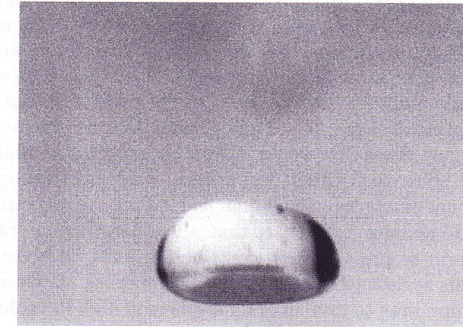

Plate 12. Oscillating water drops of $a_0 = 3.5$ mm, freely suspended in the vertical air stream of a wind tunnel; observation is taken from below the drop's equator.
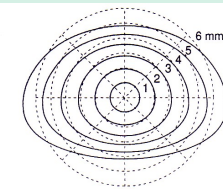

Fig. 10-15: Shape of water drops in air, computed by the method of Bashford and Adams 1883, for equivalent drop diameters (D_0) of 1 to 6 mm, for 1 atm and 20°C. Shown for comparison are circles (dashed) of equivalent diameters 1 to 6 mm. (From Beard and Chuang, 1987; by courtesy of the Am. Meteor. Soc., and the authors.)
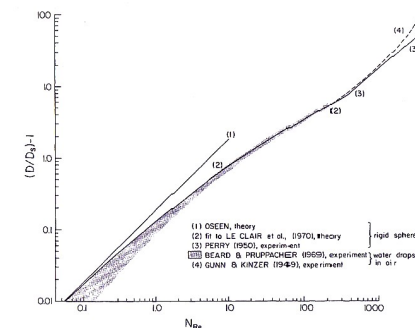
oscillation.

Fig. 10-8: Comparison between the Reynolds number dependence of the dimensionless drag, D/D_S, for rigid spheres and liquid circulating water drops.

Exercise:

- Estimate the falling velocity for droplets with diameter of 10 μm, 100 μm, 1 mm, 5 mm, respectively, using the following formulae. Assume $\rho_{air}/\rho_l=10^{-3}$

$$V(r) = aD^b (\rho_{air} / \rho_l)^{1/2}$$

$$a = 2115 \ cm^{1-b} s^{-1}$$

$b = 0.8$, b = 0.5 for large drops

D : *diameter* of a raindrop in μm

- Example of Solution

$2. \, D = 100 \, \mu\text{m}$

$$V(r) = aD^b (\rho_{air} / \rho_l)^{1/2} = 2115cm/s\left(\frac{100}{2115}\right)^{0.8}(10^{-3})^{1/2}$$

$= 21.15 \text{ m/sX0.09X3.16X0.1} = 0.58\text{m/s}$

$a = 2115 \, cm^{1-b}s^{-1}$

$b = 0.8,$

$D = 100 \, \mu\text{m}$

Breakup of raindrops:

- *When r > 3.5 mm, breakup becomes noticeable.*
  - *The probability of breakup per unit time:*

    $$P_B(m) = 2.94 \times 10^{-7} \exp(3.4R)$$

    R : radius of drop with mass m in mm
  - *The number of drops with mass m to m+dm formed by the breakup of one drop of mass m$'$*

    $$Q_B(m', m) = 0.1 \cdot R'^3 \cdot \exp(-15.6R)$$

    R' : radius of break up drop

    R : radius of newly formed drops

  - *The net production of drops of mass m by breakup:*

    $$\left(\frac{\partial N(m,t)}{\partial t} \right)_{bre} = -N(m,t)P_B(m) + \int_m^\infty N(m',t)Q_B(m',m)P_B(m')dm'$$

    Loss of droplets   New droplets
    due to breakup   formed by breakup

Cold (ice) Cloud/Precipitation Microphysics:

- Most of precipitation, especially heavy rainfall, is produced by cold cloud process.

- Main processes control growth of cold cloud/precipitation droplets:

Homogeneous: Deposition of vapor on ice, occurs in cirrus clouds or near top of deep convection and stratiform clouds, < -36°C for droplets 20-60μm.

Heterogeneous: produce most of ice mass and precipitation

Riming: supercool water deposit on ice, 0 ° C- -40 ° C, can produce grauple and hails.

aggregation: merging between ice particles and snow flakes

Depositional growth:

•Super-saturation, S_i, is easier to reach for ice than for liquid droplets

$$e_s = e_o \cdot \exp\left(\frac{L}{R_v} \cdot \left(\frac{1}{T_o} - \frac{1}{T}\right)\right)$$

$L_i < L_l$, thus $e_{s,i} > e_{s,l}$

At T= -10C, $S_l=0$, $S_i=10\%$

At T= -20C, $S_l=0$, $S_i=21\%$

• Growth rate of an ice particle

$$\frac{dm}{dt} = \frac{4\pi\tilde{C}\tilde{S}_i}{F_{ki} + F_{Ci}}$$

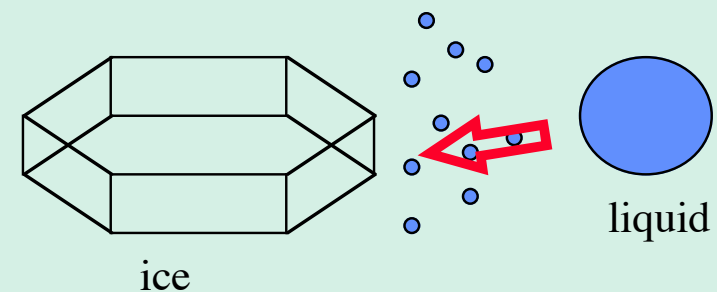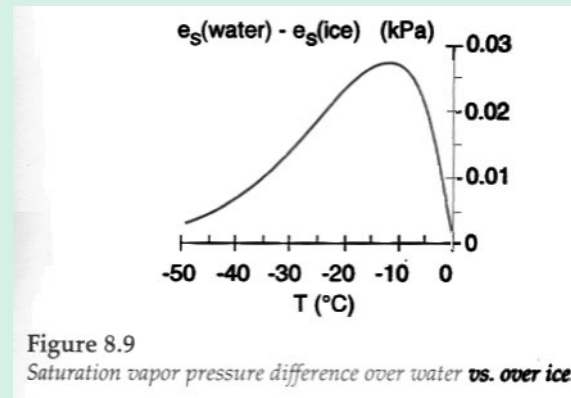$\tilde{C}$: shape factor of ice particle

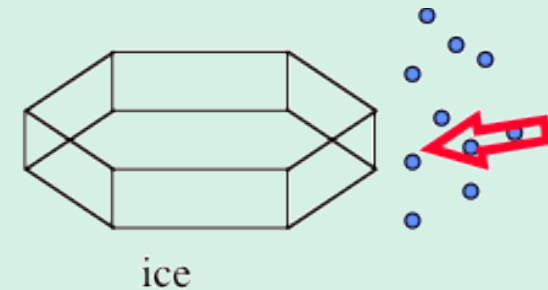$\tilde{S}_i$ ambinet supersaturation for ice

$F_{Ki} \equiv$ heat conductivity of ice particle

F_{Di} vapor diffusivity

$$\frac{dm}{dt} = \frac{4\pi\tilde{C}\tilde{S}_i V_F}{F_{ki} + F_{Di}}$$

For a falling ice particle

V_F : *ventilation* factor

ice

e_S(water) - e_S(ice) (kPa)

Figure 8.9
Saturation vapor pressure difference over water *vs. over ice.*

ice

liquid

Ice crystals grow by taking water molecules away from liquid drops.

Wegener-Bergeron-Findeisen Process

Shape of ice crystals-habit

•*The shape change with increasing super-saturation is to maximize the surface on which the increased ambient vapor can deposit.*

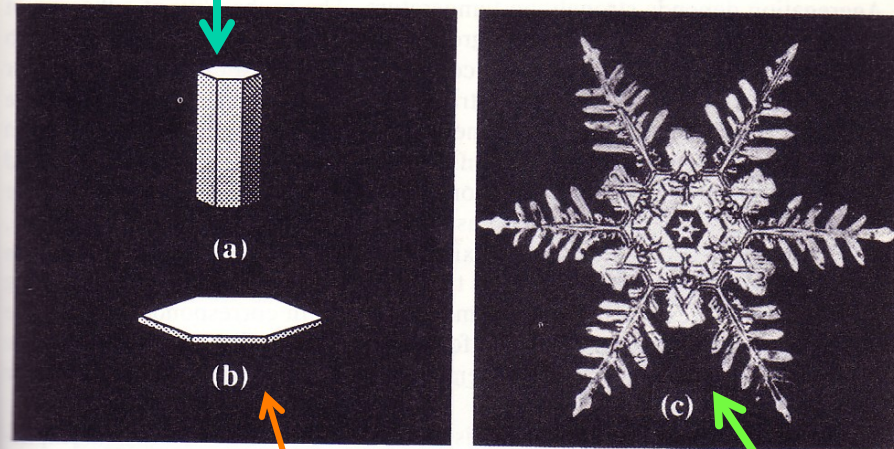-4C ~ -10C, -22C ~ -50C
Needles, hollow column

Figure 3.8 Schematic representation of the main shapes of ice crystals: (a) columnar, or prismlike; (b) plate; (c) dendrite. (Adapted from Rogers and Yau, 1989.)

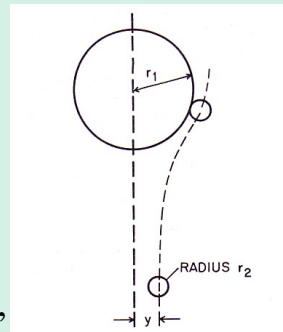-4C ~ 0C, -10C ~ -22C
Hexagonal plate, sector plates, dendrites

-12C ~ -16C
dendrites

Aggregation and Riming

- Aggregation: merging between ice crystals. Aggregation produce snow flakes.

ice crystals

$$\frac{dm}{dt}\bigg|_{col} = A_m \left| V(m) - V(m') \right| \rho_l q_{m'} \sum_c (m,m')$$

$$\sum_c (m,m') \propto \frac{y^2}{(r_1 + r_2)^2}, \; collection \; \text{efficiency,}$$

A_m : effective cross-section area, depends on the shape of the ice crystal.

V : fall speed

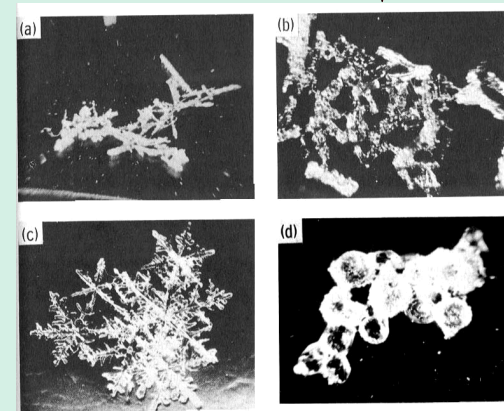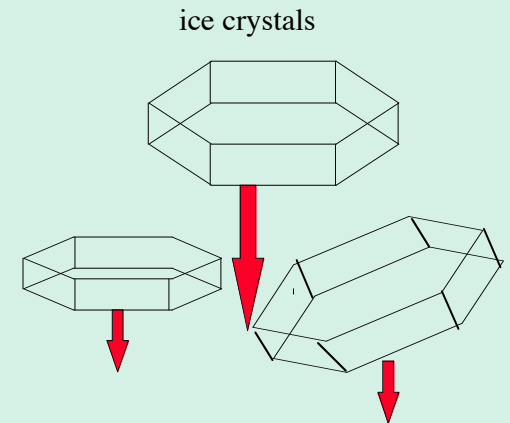$\rho q_{m'}$: liquid water content of the collected drops

Fig. 4.36 Aggregates of (a) densely rimed needles; (b) unrimed to moderately rimed columns; (c) dendrites; (d) unrimed to densely rimed frozen drops. (Courtesy Cloud Physics Group, University of Washington.)

- Collection efficiency for ice crystals depends on temperatures, often assumed to increase exponentially with temperature. It peaks at 0C ~ -5C and also shows a secondary peak at –10C ~ –16C. Aggregation stops below –20C.
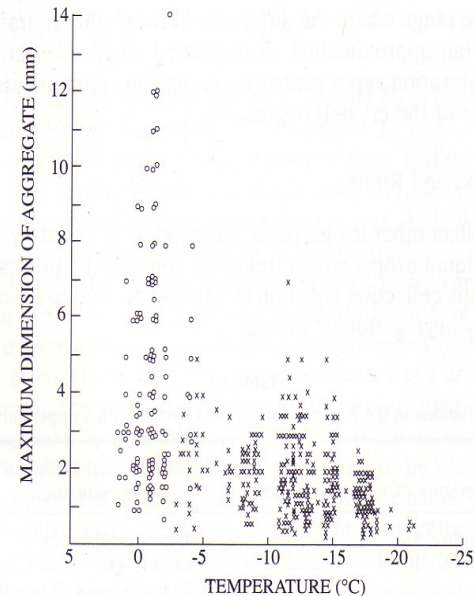
Figure 3.9 Maximum dimensions of natural aggregates of ice crystals as a function of the temperature of the air where they were collected. × indicates crystals collected from an aircraft. Circles represent crystals collected on the ground. (From Hobbs, 1973b. Reprinted with permission from Oxford University Press.)

- Shape also affect the growth rate.
  - Collection efficiency of broad-branched crystal is lower than that of a hexagonal plate of the same Reynolds number, partically because of its smaller effective cross-section area.
  - Terminal velocity of dendrites and powder snow is approximately independent of its size. Whereas the terminal velocity of rimed crystals and needles flakes strongly vary with their sizes.
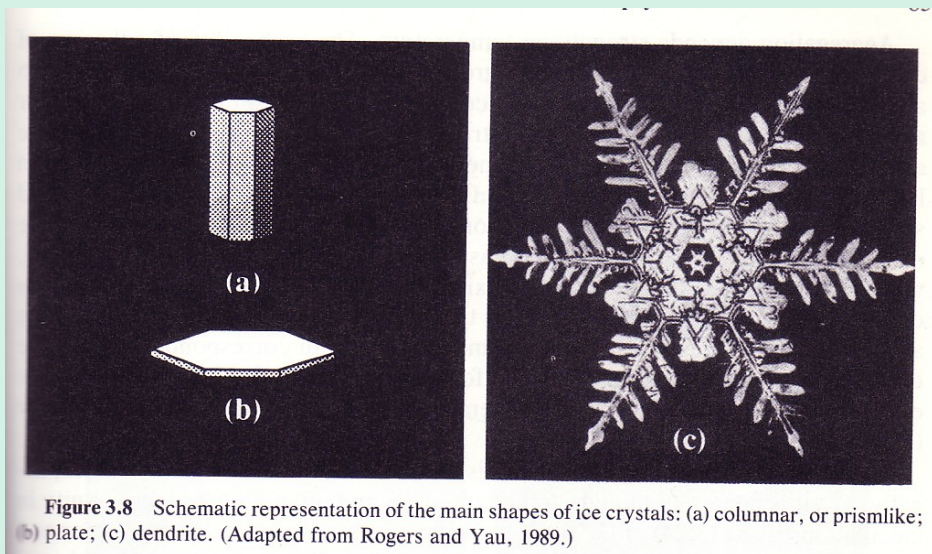
Figure 3.8 Schematic representation of the main shapes of ice crystals: (a) columnar, or prismlike; (b) plate; (c) dendrite. (Adapted from Rogers and Yau, 1989.)

- Riming-formation of hails:
  - Supercool water droplets collide with ice crystals and instantly freeze on the surface of the ice crystals.
  - Riming can produce snow flakes, graupels and hailstones.
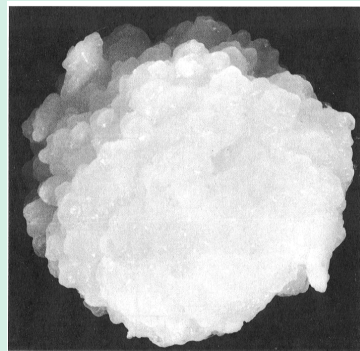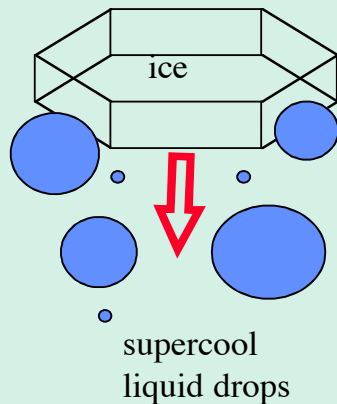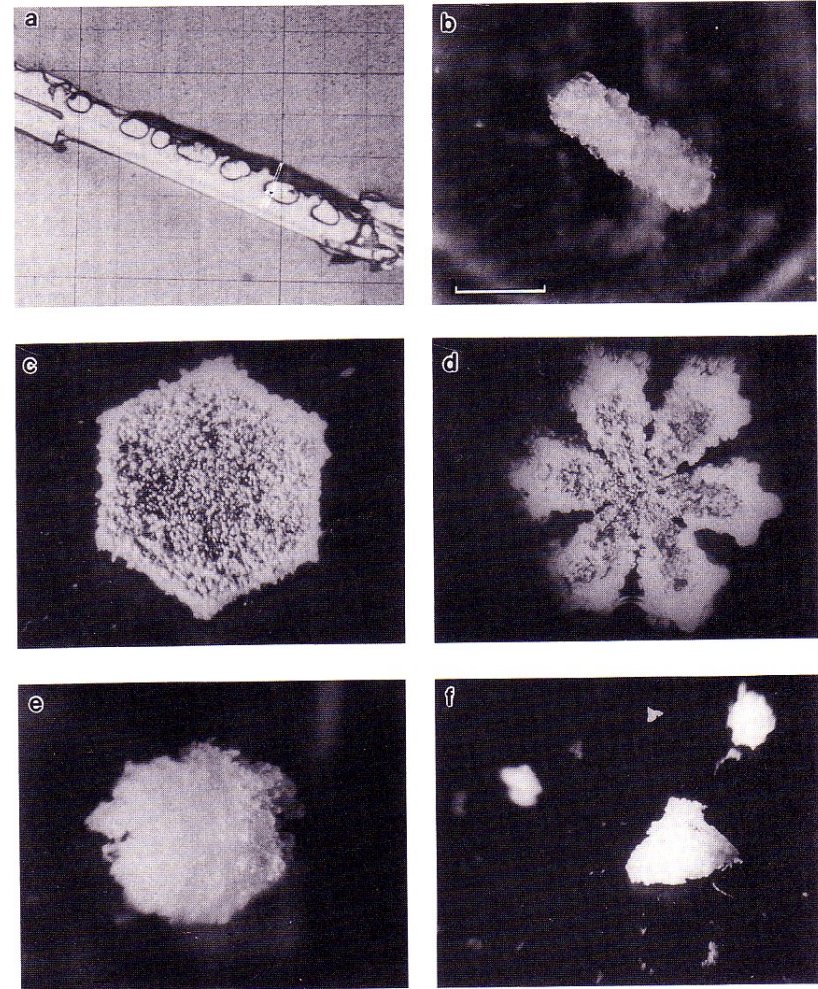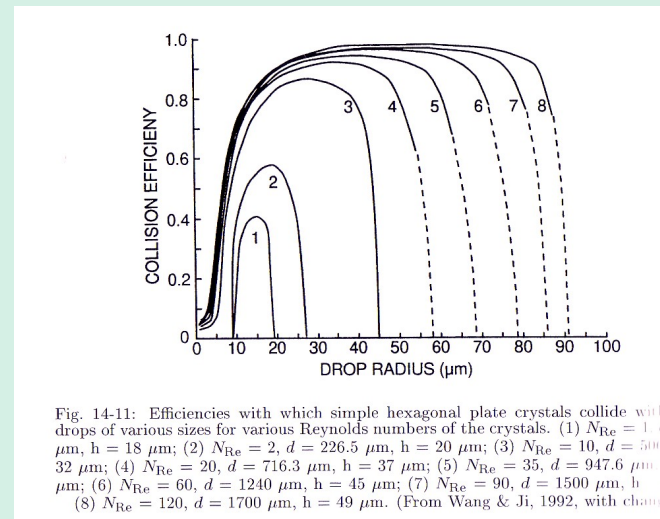

ice

supercool liquid drops

Fig. 4.35 Artificial hailstone, actual size, showing lobe structure. Growth was initially dry but tended toward wet growth as the stone grew. [From *Quart. J. Roy. Met. Soc.* **94**, 10 (1968).]
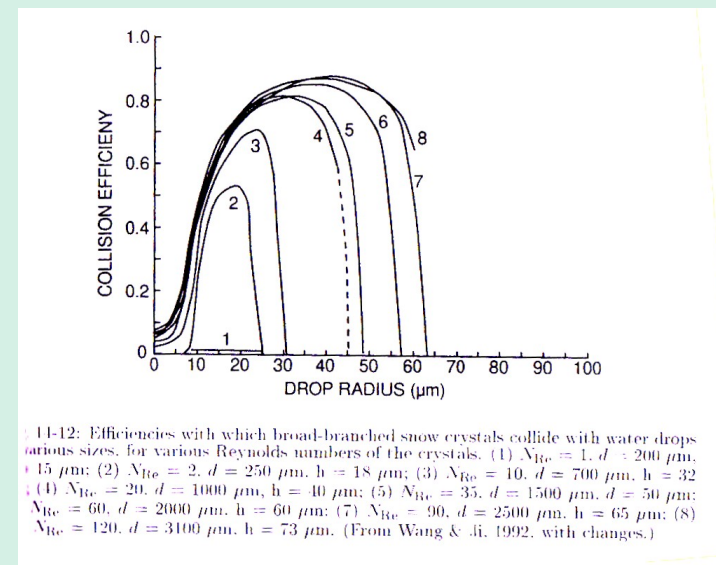

Figure 3.10 (a) A lightly rimed needle; (b) densely rimed column; (c) densely rimed plate; (d) densely rimed stellar; (e) lump graupel; (f) cone graupel. (From Wallace and Hobbs, 1977.)

- Shape of ice crystals also affect the riming growth rate.
  - Similar to aggregation process, collection efficiency of broad-branched crystal is lower than that of a hexagonal plate of the same Reynolds number, due to its smaller effective cross-section.
  - Minimum cut-off size of snow crystals for riming varies with shapes. Generally about 100-200 μm for planar snow crystals, and 35μm for columnar crystals.

Fig. 14-11: Efficiencies with which simple hexagonal plate crystals collide with drops of various sizes for various Reynolds numbers of the crystals. (1) $N_{Re} = 1$, d μm, h = 18 μm; (2) $N_{Re} = 2$, d = 226.5 μm, h = 20 μm; (3) $N_{Re} = 10$, d = 500, 32 μm; (4) $N_{Re} = 20$, d = 716.3 μm, h = 37 μm; (5) $N_{Re} = 35$, d = 947.6 μm, μm; (6) $N_{Re} = 60$, d = 1240 μm, h = 45 μm; (7) $N_{Re} = 90$, d = 1500 μm, h (8) $N_{Re} = 120$, d = 1700 μm, h = 49 μm. (From Wang & Ji, 1992, with changes.)

Riming of hexagonal crystals

14-12: Efficiencies with which broad-branched snow crystals collide with water drops various sizes, for various Reynolds numbers of the crystals. (1) $N_{Re} = 1$, d = 200 μm, 15 μm; (2) $N_{Re} = 2$, d = 250 μm, h = 18 μm; (3) $N_{Re} = 10$, d = 700 μm, h = 32 (4) $N_{Re} = 20$, d = 1000 μm, h = 40 μm; (5) $N_{Re} = 35$, d = 1500 μm, d = 50 μm; $N_{Re} = 60$, d = 2000 μm, h = 60 μm; (7) $N_{Re} = 90$, d = 2500 μm, h = 65 μm; (8) $N_{Re} = 120$, d = 3100 μm, h = 73 μm. (From Wang & Ji, 1992, with changes.)

Riming of broad-branched crystals

Fall speed

- Graupels and colunmar crystals: fall speed increases rapidly with their sizes. Gravitational force ($\sim r^3$) increases more than drag force proportional to the cross-section area (r^2).

- Planar crystals: fall speed varies little with size. Gravitational force ($\sim r^2$) increases at a similar rate of the drag force ($\sim$cross-section area, r^2).
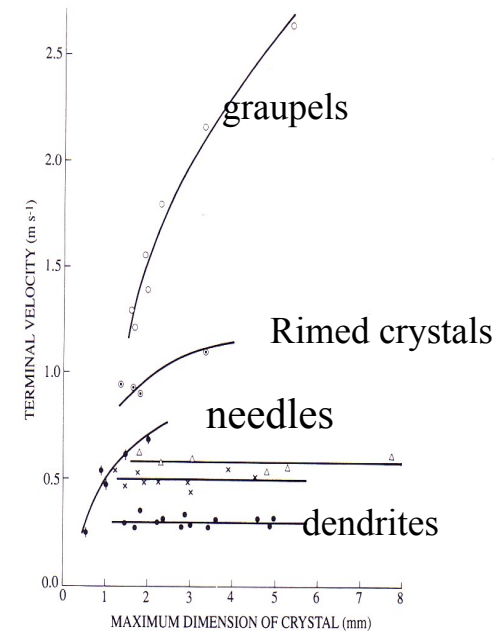
Figure 3.12 Terminal fall speeds of snow crystals as a function of their maximum dimensions. Open circle (uppermost curve) indicates graupel fall speeds. Other curves are for rimed crystals (dot in circle), needles (filled circle with slash), spatial dendrites (triangle), powder snow ($\times$), and dendrites (filled circle). (From Nakaya and Terada, 1935.)

oscillation.
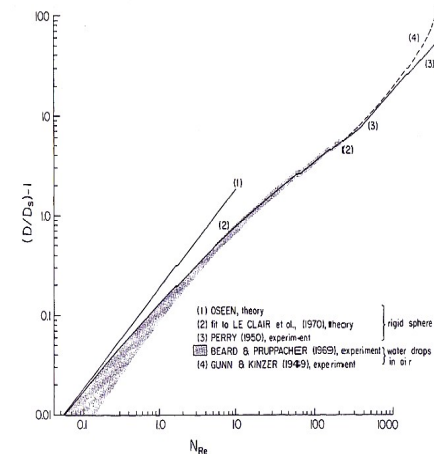
Fig. 10-8: Comparison between the Reynolds number dependence of the dimensionless drag, D/D_S, for rigid spheres and liquid circulating water drops.

Melting:

- Above melting zone (T($\propto$)<0°C), melting can occur on the surface of hailstone when T(R) $\geq$ 0C, determined by

$$\frac{dm}{dt}_{col}\left[L_i - c_w(T(R) - T_w)\right] + 4\,\pi R D_v\left[\rho_v(\infty) - \rho_v(R)\right]V_{Fs}\,L_i$$

net heat gain *by* the ice crystal
by freez of liquid water and
heat transfer from liquid to ice

diffusion of heat toward
the ice by vapor deposition

Heat gain by ice

$$= 4\,\pi R K_a\left[T(R) - T(\infty)\right]V_{FC}$$
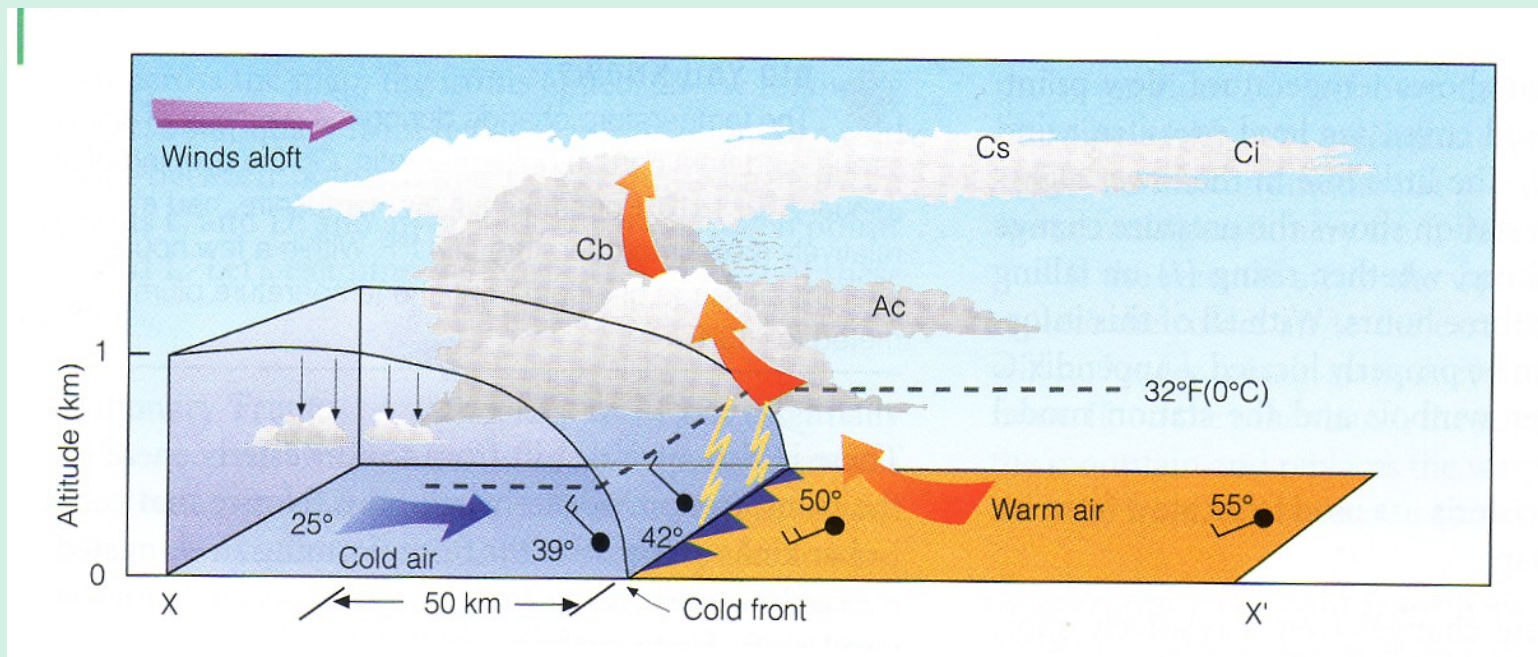
diffusion of heat away from
the ice

Heat lost by ice

K_a : thermal conductivity of air

V_{FC} : ventilation factor for conduction

c_W : specific heat of water

D_v : diffusivity of vapor
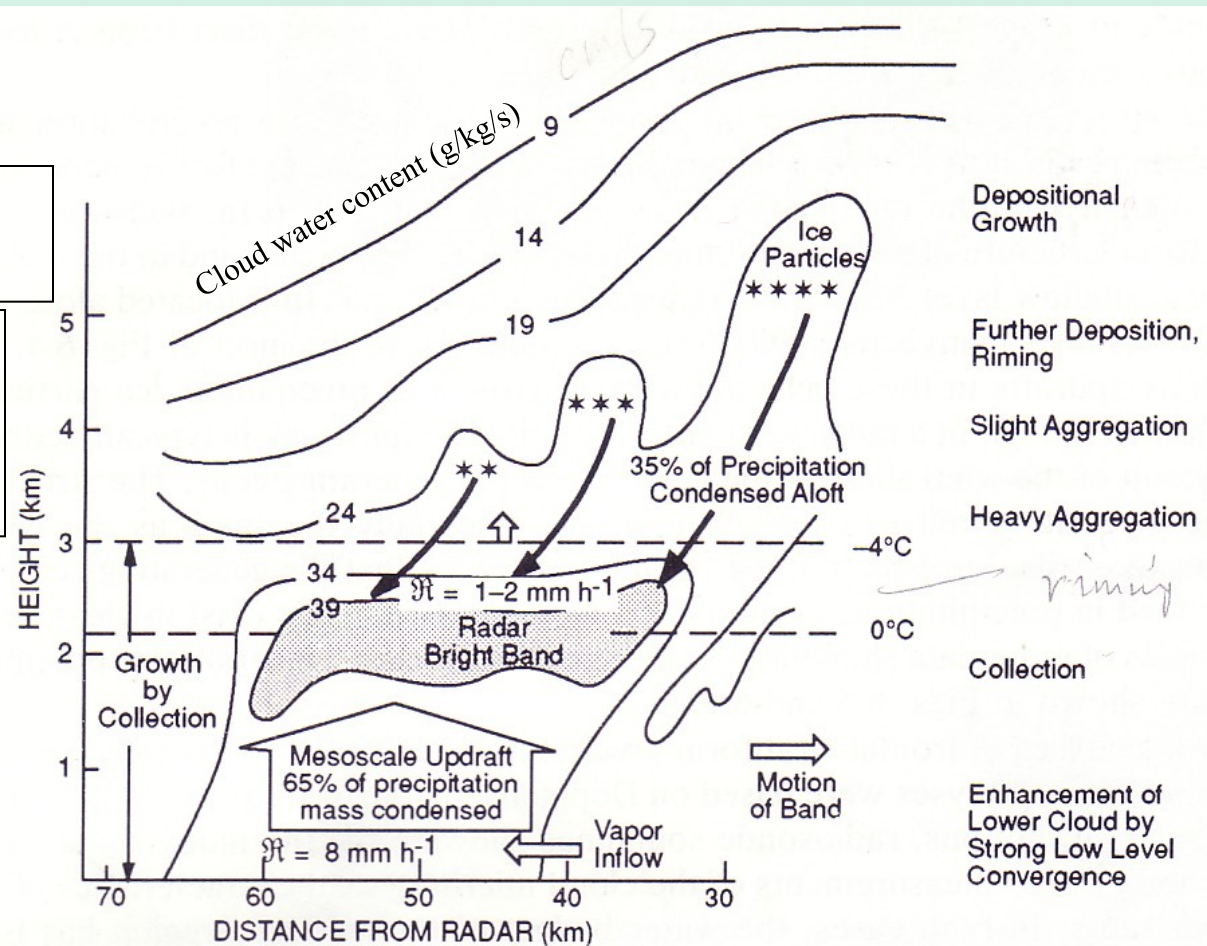
- T(R) $\geq$ 0C: wet growth; T(R) < 0C: dry growth

Formulas are not required for GEO 347P.

Melting:

- As ice fall into the area where T($\propto$)>0°C, melting begins:

$$-L_i \frac{dm}{dt}_{mel} = 4\pi R K_a \left[T(\infty) - 273K \right] V_{FC} + \frac{dm}{dt}_{col} c_w (T_w - 273K)$$

latent cooling of melting   *diffusion* of heat toward the ice from ambient air   *heat* transfered to ice from water drops collected ice particle

$$+ 4\pi R D_v \left[\rho_v(\infty) - \rho_v(R) \right] V_{Fs} L_i$$

diffusion of heat toward the ice by vapor

K_a : thermal conductivity of air

V_{FC} : ventilation factor for conduction

c_W : specific heat of water
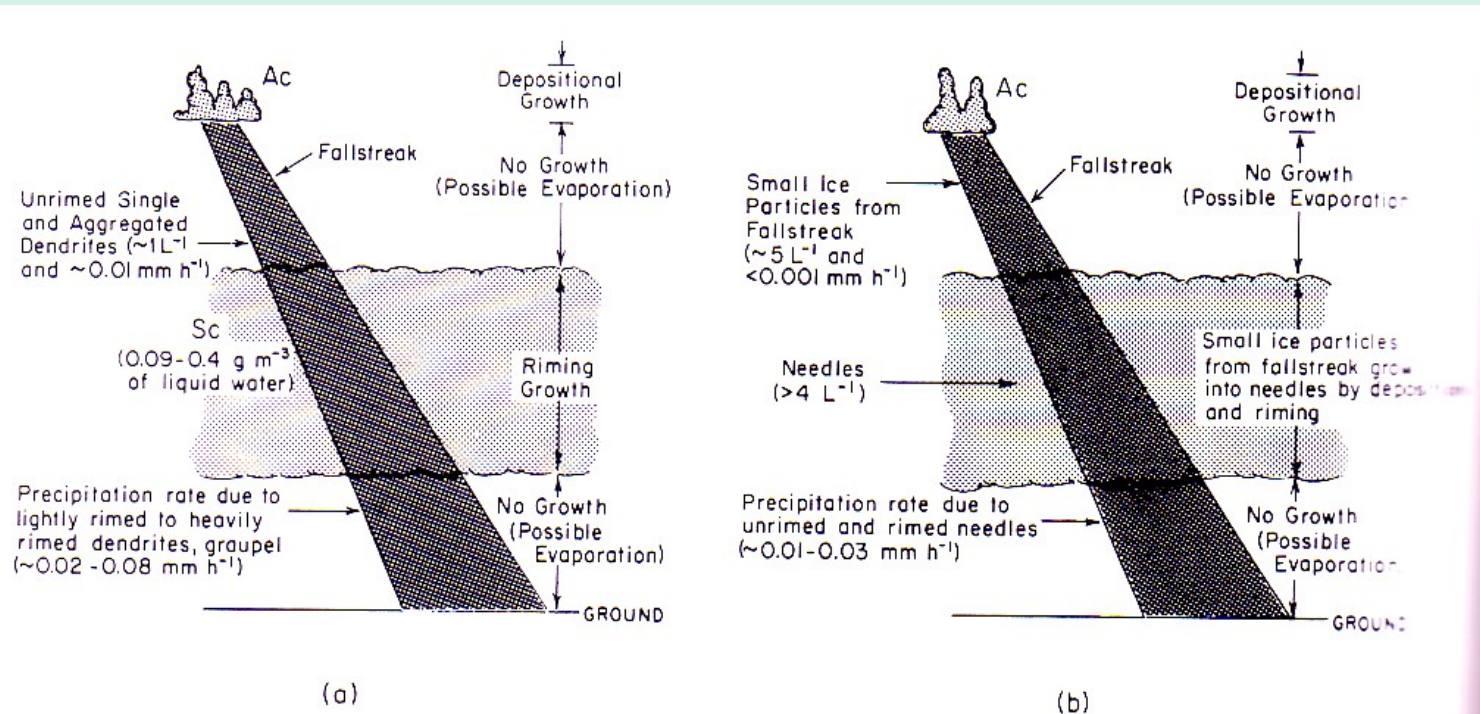
D_v : diffusivity of vapor

Cloud Dynamics:

Cloud microphysical process in real clouds:

"seeder zone"
(~20% of rainfall)

Feeder zone (~80% of rainfall)
Mainly deep Stratiform cloud

Melting band (~0%)

Rain **region** (0%)

Figure 6.8 Schematic of the dynamical and microphysical processes in a stratiform frontal rainband over western Washington State. (From Houze *et al.*, 1981.)
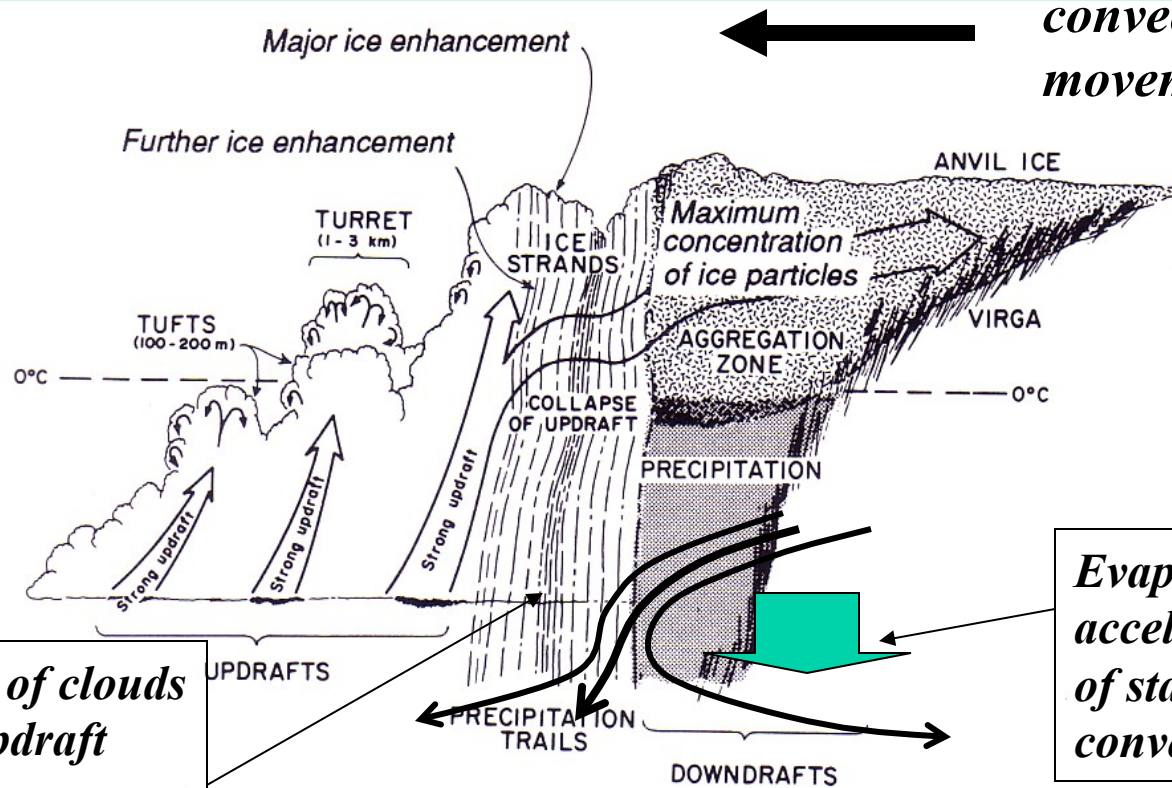
Interaction between cloud microphysical processes:

Figure 5.46 Schematic of interaction of altocumulus and stratocumulus clouds. (a) Dendrite crystals in a fallstreak from the altocumulus fall into the stratocumulus, where they grow by riming and reach the ground as light precipitation. (b) Small ice particles in a fallstreak from the altocumulus grow into needles in the stratocumulus and contribute to the precipitation at the ground. (From Locatelli et al., 1983. Reproduced with permission from the American Meteorological Society.)

Ice crystals fall from altocumulus grow by riming in stratocumulus below and produce precipitation. A_c and S_c alone would not produce precipitation.

Interaction between cloud microphysics and dynamics:
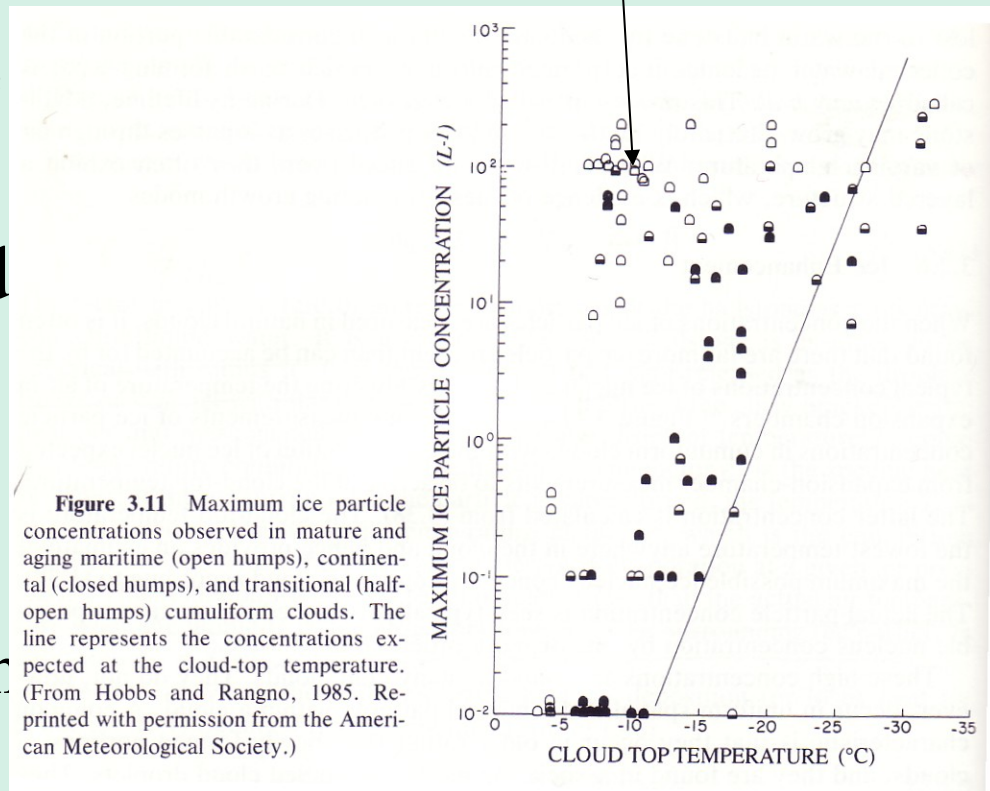

Direction of convection movement

Major ice enhancement

Further ice enhancement

ANVIL ICE

TURRET (1 - 3 km)

Maximum concentration of ice particles

ICE STRANDS

TUFTS (100 - 200 m)

AGGREGATION ZONE

VIRGA

0°C

Strong updraft

COLLAPSE OF UPDRAFT

0°C

PRECIPITATION

Evaporative cooling accelerate downdraft of stable air, putting convection forward

Downdrafts of clouds drops kill updraft

UPDRAFTS

PRECIPITATION TRAILS

DOWNDRAFTS

Figure 8.1 Empirical model of a small cumulonimbus cloud. Based on about 90 research aircraft penetrations of small cumulonimbus and large cumulus clouds. (From Hobbs and Rangno, 1985. Reprinted with permission from the American Meteorological Society.)
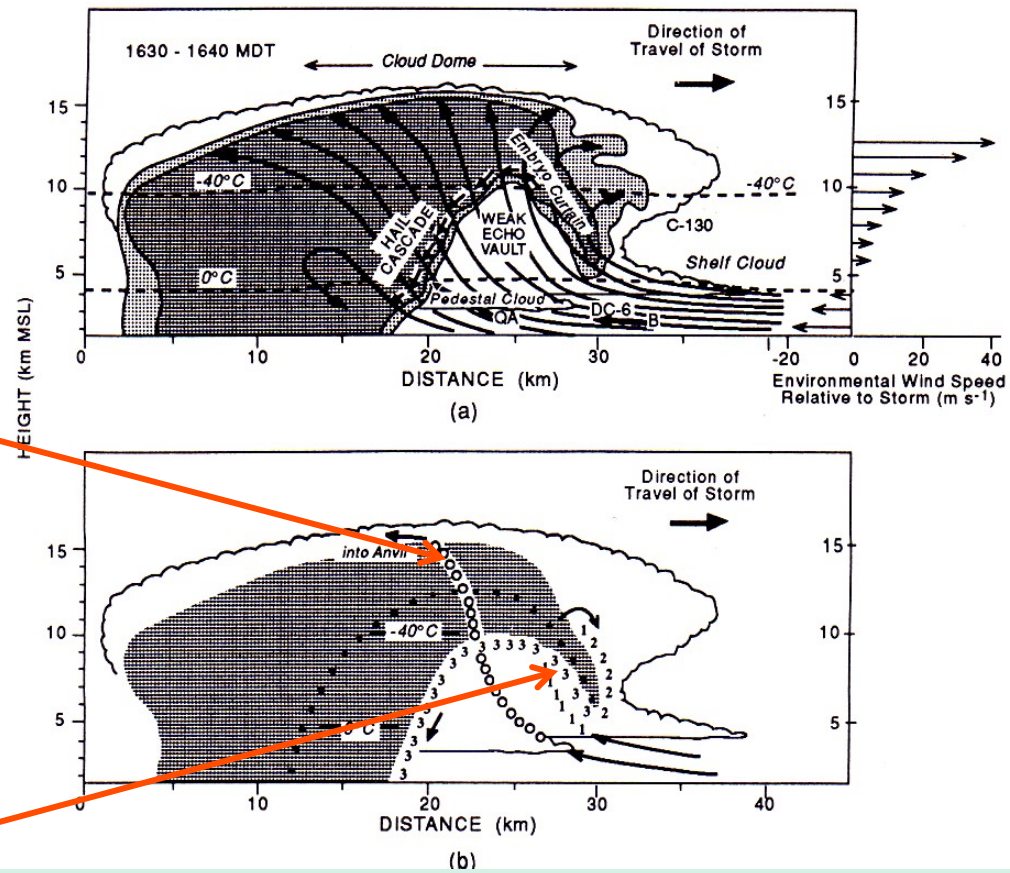
Ice enhancement

Possible causes:

- Fragmentation of ice crystals

- Ice splinter produced in riming

- Contact nucleation
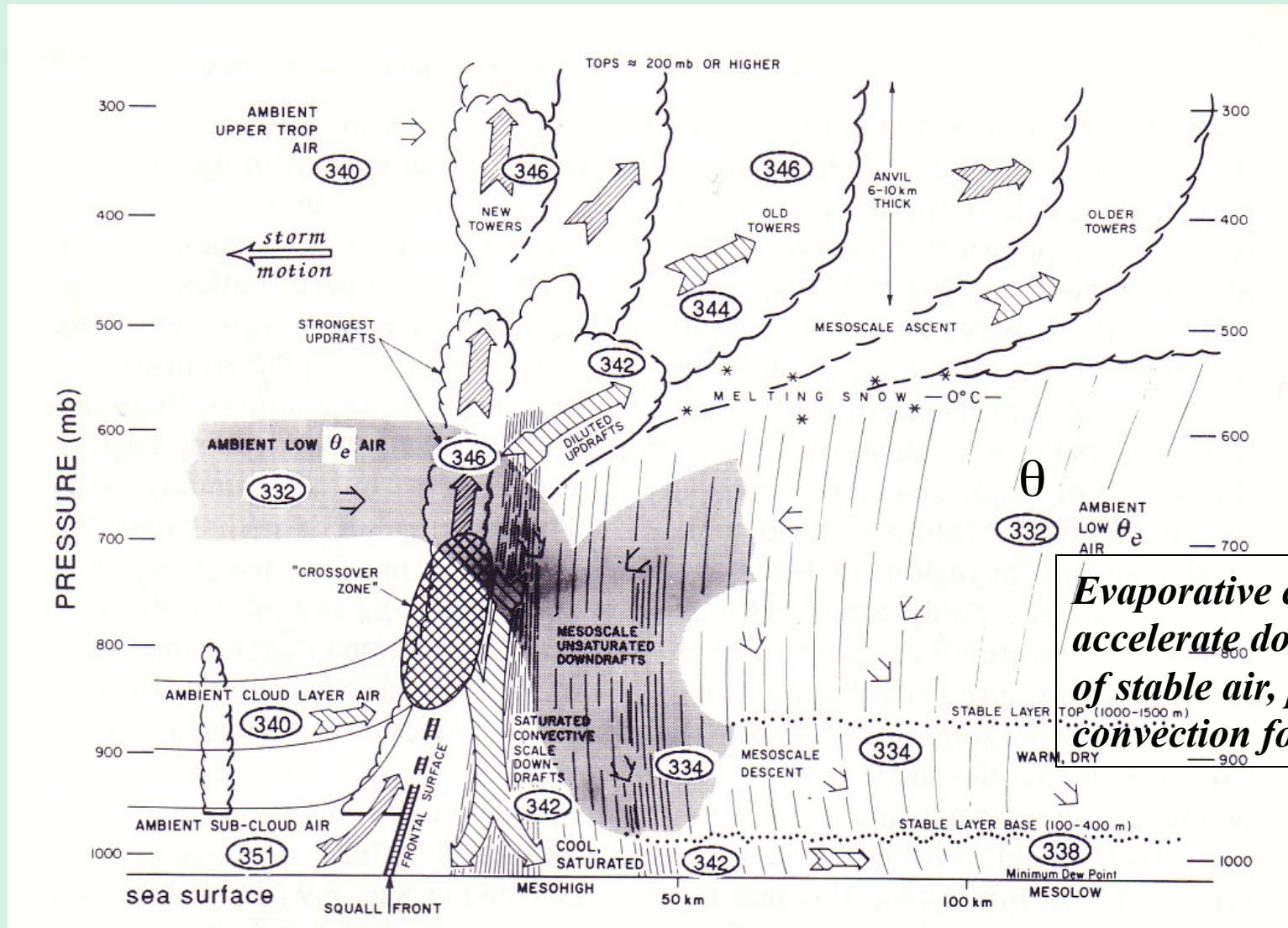
- Condensation or deposition uncleation

Figure 3.11 Maximum ice particle concentrations observed in mature and aging maritime (open humps), continental (closed humps), and transitional (half-open humps) cumuliform clouds. The line represents the concentrations expected at the cloud-top temperature. (From Hobbs and Rangno, 1985. Reprinted with permission from the American Meteorological Society.)

Cloud droplets being rapidly lifted to anvils and detrained out of convection

Repeat circulation in convection forms graupels and hails.

Figure 8.12 (a) Vertical cross section of cloud and radar echo structure of a supercell thunderstorm in northeastern Colorado. The section is oriented along the direction of travel of the storm, through the center of the main updraft. Two levels of radar reflectivity are represented by different densities of hatched shading. The locations of four instrumented aircraft are indicated by C-130, QA, DC-6, and B. Bold arrows denote wind vectors in the plane of the diagram as measured by two of the aircraft (scale is only half that of winds plotted on right side of diagram). Short thin arrows skirting the boundary of the vault represent a hailstone trajectory. The thin lines are streamlines of airflow relative to the storm. To the right is a profile of the wind component along the storm's direction of travel. (b) Vertical section coinciding with (a). Cloud and radar echo are the same as before. Trajectories 1, 2, and 3 represent three stages in the growth of large hailstones. The transition from stage 2 to stage 3 corresponds to the reentry of a hailstone embryo into the main updraft prior to a final up–down trajectory during which the hailstone may grow large, especially if it grows close to the boundary of the vault as in the case of the indicated trajectory 3. Other, less-favored hailstones will grow a little farther from the edge of the vault and will follow the dotted trajectory. Cloud particles growing within the updraft core are carried rapidly up and out into the anvil along trajectory 0 before they can attain precipitation size. (From Browning and Foote, 1976. Reprinted with permission from the Royal Meteorological Society.)
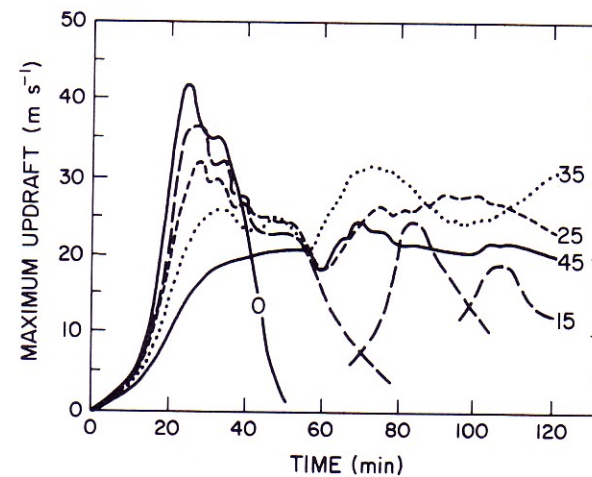
Zipser 1977

- No shear: single, short lived cumulus cell
- weak shear: multi-cells
- Stronger shear: MCC
- Strongest shear: single supercell convection

*What are the dynamic and cloud microphysical causes?*

Figure 8.15 Profiles of wind speed u used in three-dimensional model simulations of multicell and supercell thunderstorms. Profiles becomes asymptotic to u_s. (From Weisman and Klemp, 1982. Reprinted with permission from the American Meteorological Society.)

Figure 8.16 Results of three-dimensional model simulations of thunderstorms under different amounts of wind shear. The quantity plotted is the maximum vertical velocity as a function of time for different values of the wind-shear parameter u_s(m s^{-1}), which is the number plotted next to each curve. (From Weisman and Klemp, 1982. Reprinted with permission from the American Meteorological Society.)

Convective cells:

- Thermodynamics structure of the atmosphere, e.g., CAPE and CINE determine the probability of occurrence of convective cell;

- Dynamic structure determines
  - lifting air to LFC
  - Vigor and life-time
  - Movement

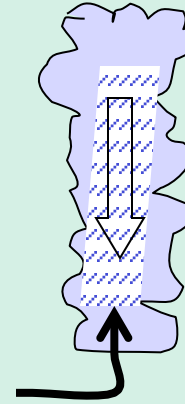Processes Convective Parameterization Schemes Emulate
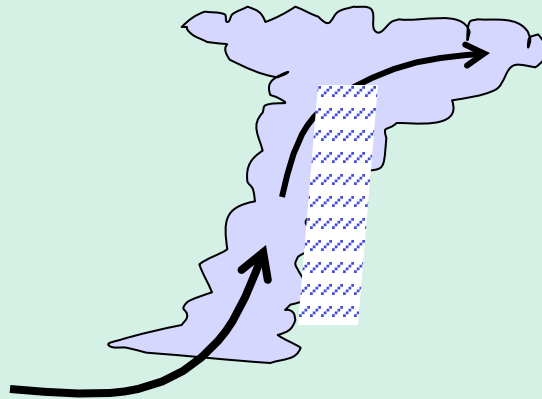
©The COMET Program
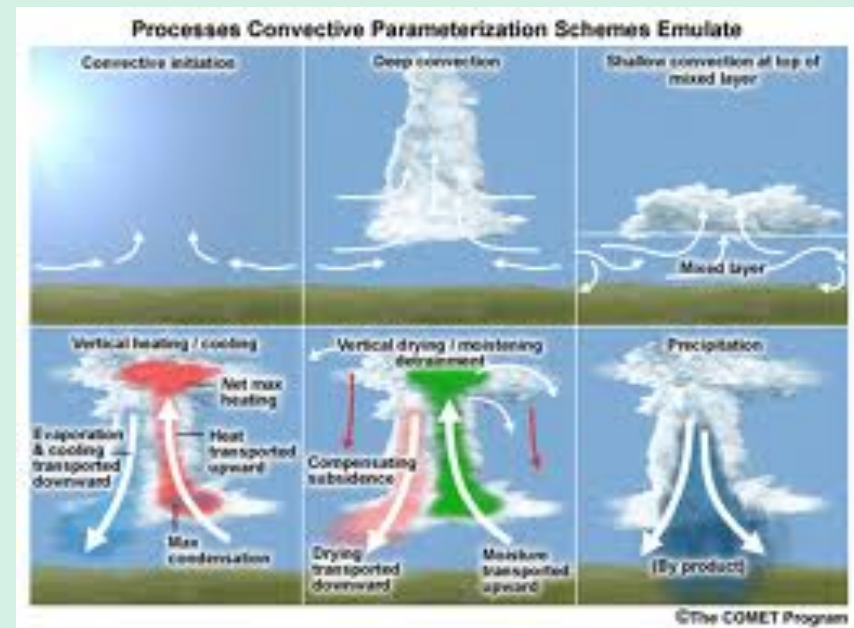
Shear instability:

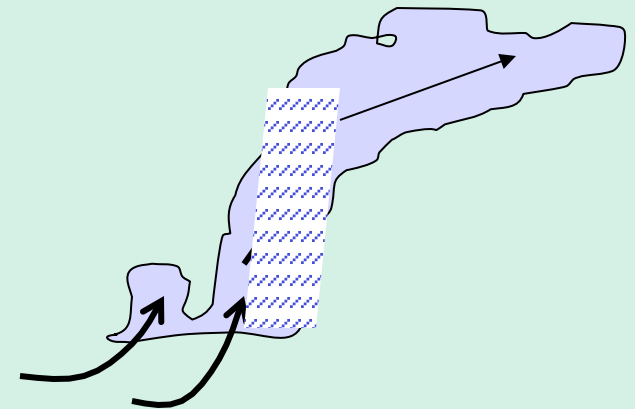$$\frac{\partial \vec{V}}{\partial z} = \frac{\partial u}{\partial z}, \frac{\partial v}{\partial z}$$
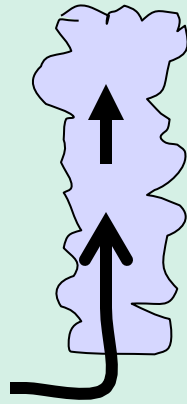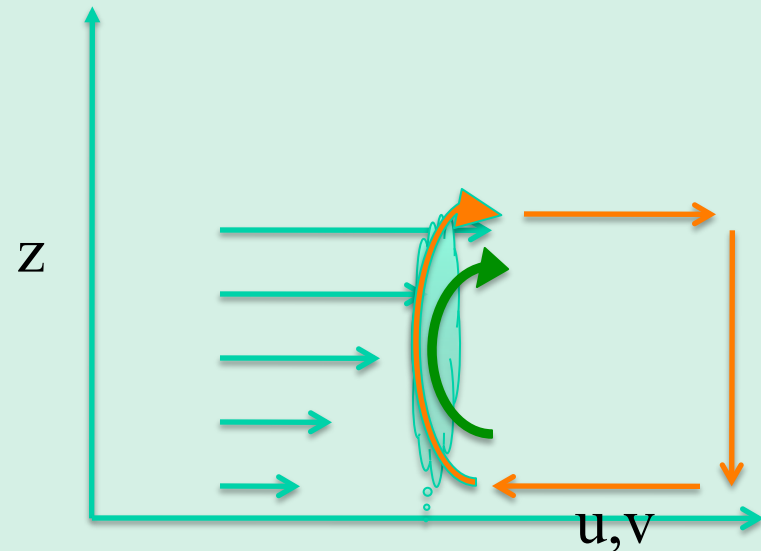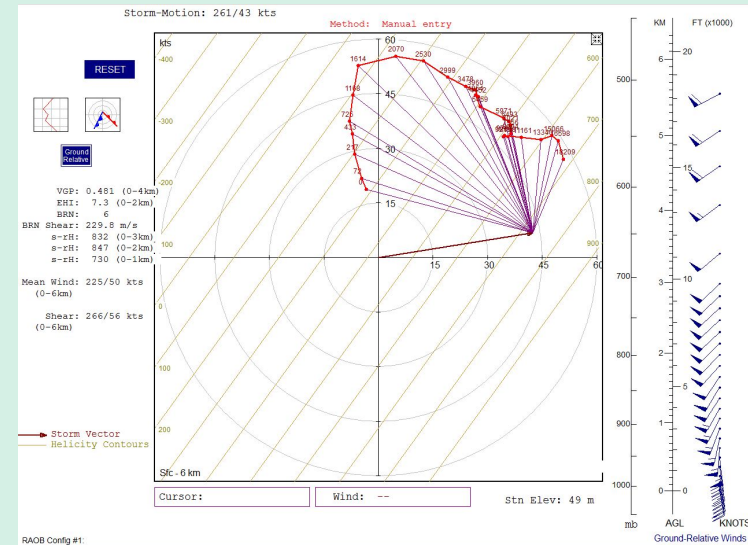
No shear

Influence the growth of the convective cells

Moderate shear

stronger shear

Influence vorticity of the convection:

- Convection prefer cyclonic flow (counter-clockwise in NH, clockwise in SH), which stretches vortex and promote rising motion.
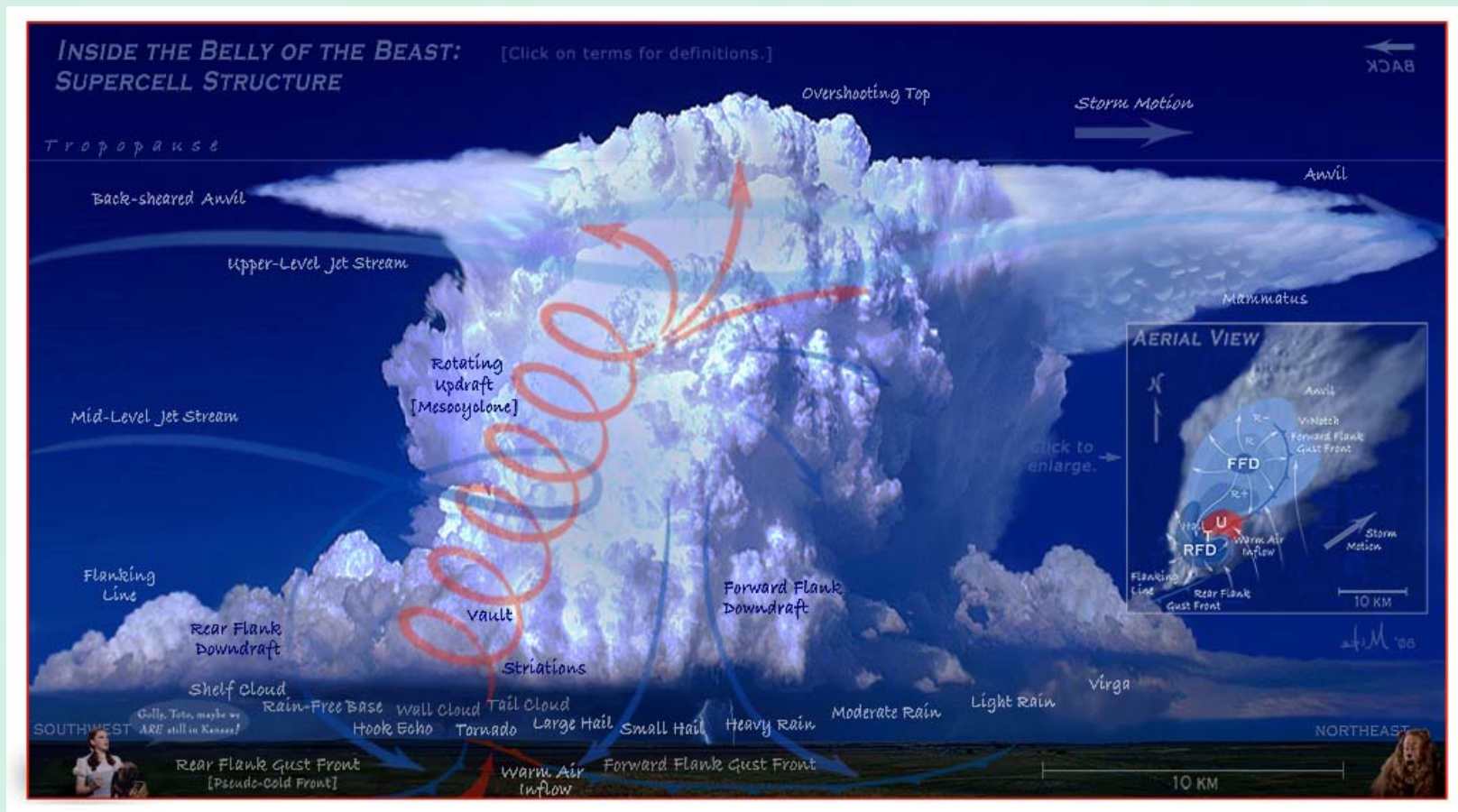
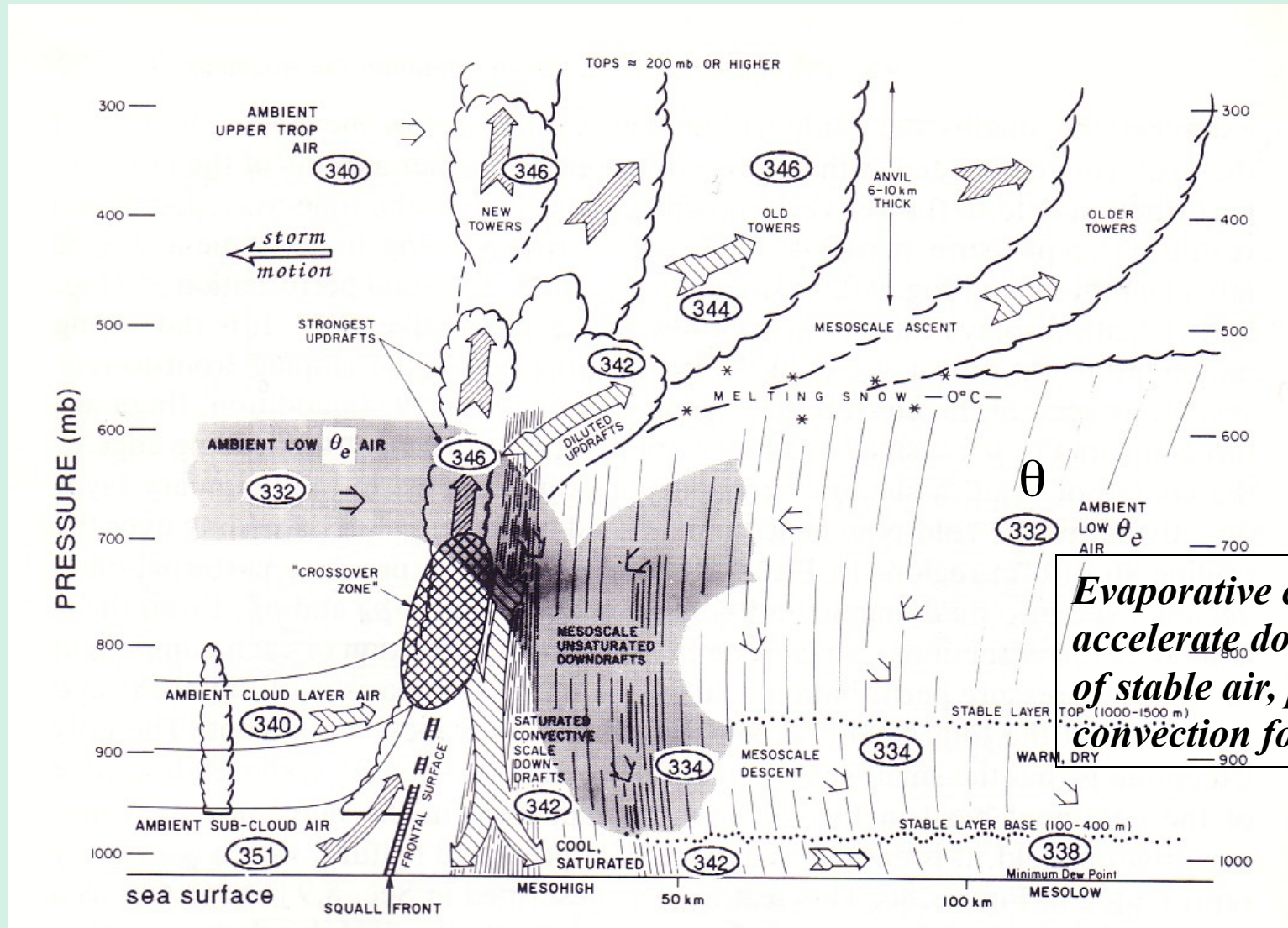Thus, $\dfrac{\partial u}{\partial z}$ or / and $\dfrac{\partial v}{\partial z} > 0$

enhances convection

Mesoscale convective systems:

Zipser 1977
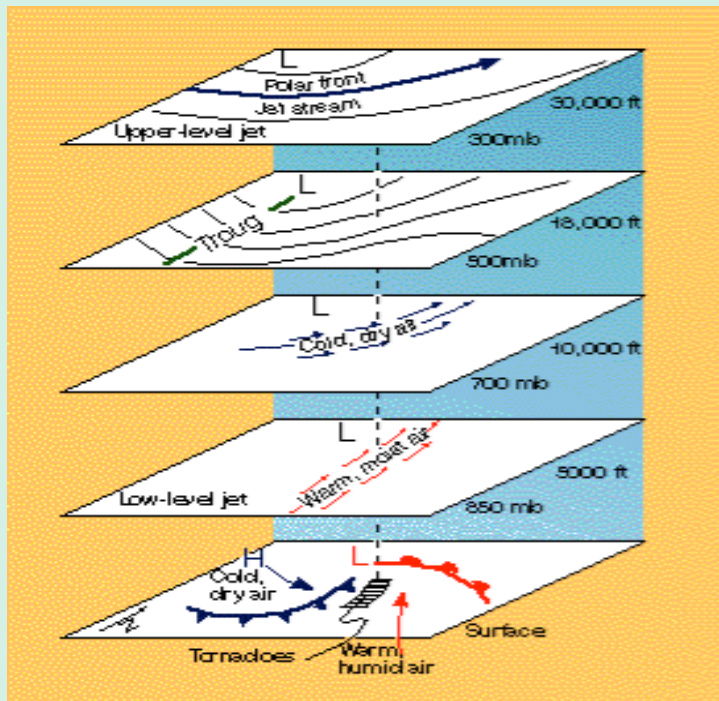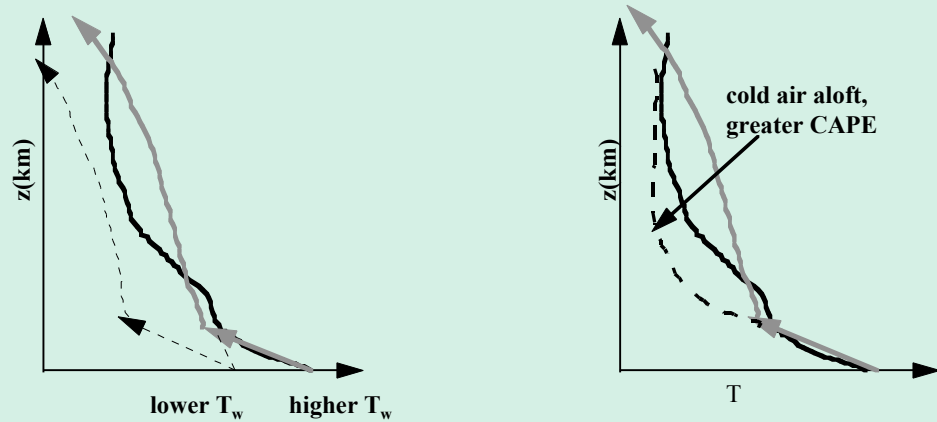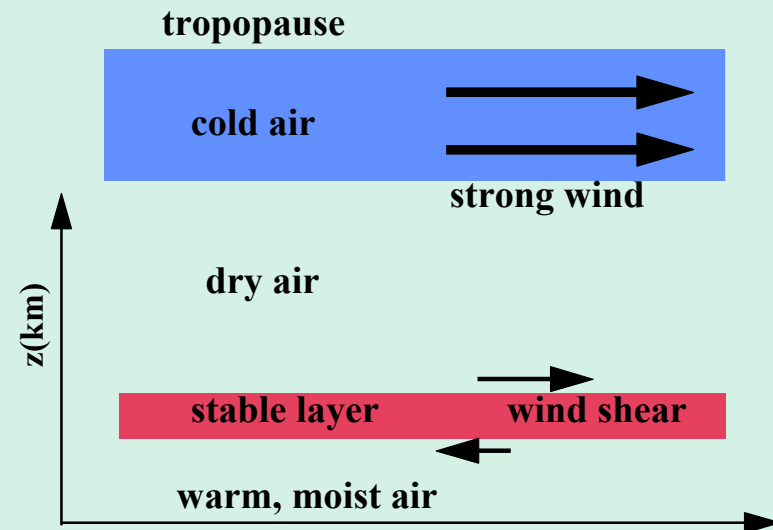
Condition for generating strong mesoscale convection:

- *Unstable lapse rate, high humidity*
- *Near the jets core*
- *Trough titled westward with height, surface low to the east of upper-level trough*
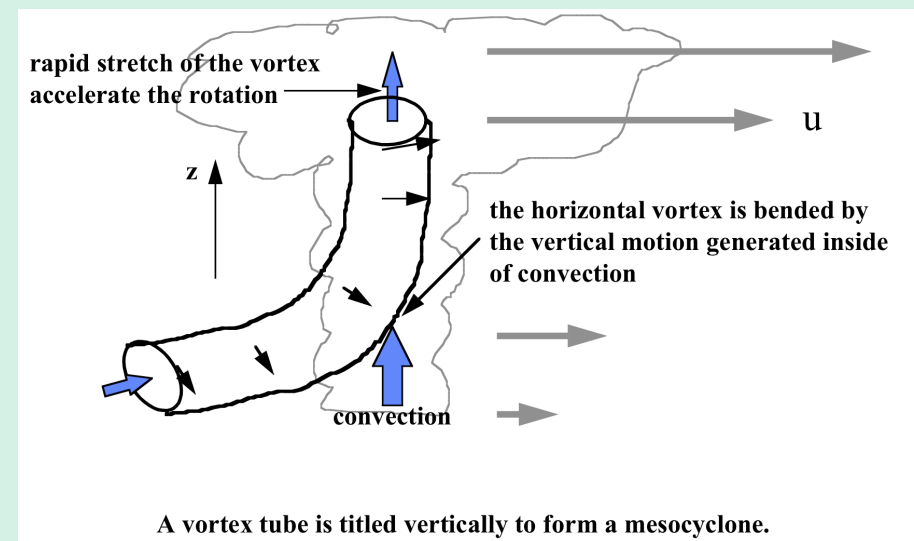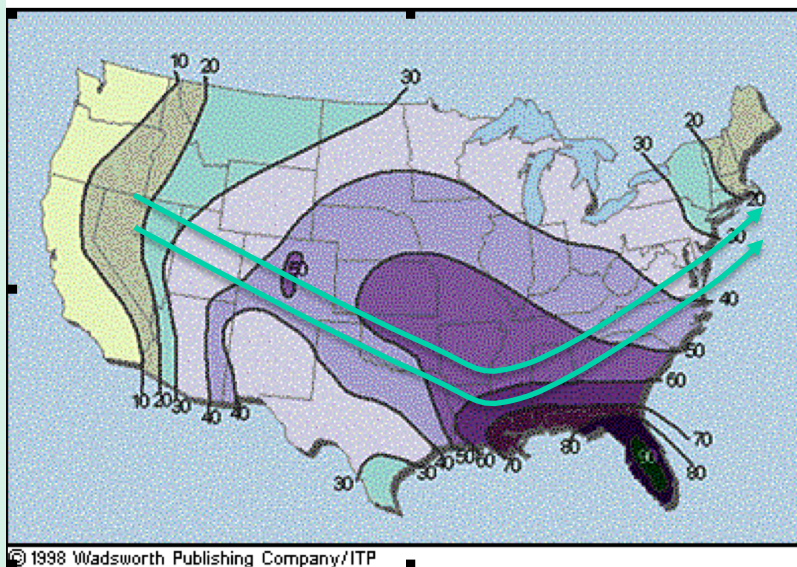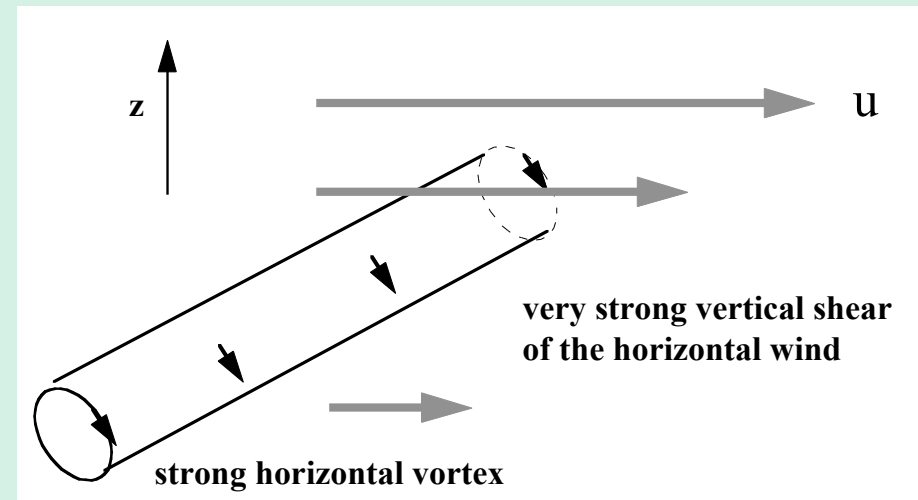

z(km)

lower T$_w$ higher T$_w$

z(km)

cold air aloft, greater CAPE

T

L
Polar front
Jet stream
Upper-level jet
300mb
30,000 ft

L
Trough
500mb
18,000 ft

L
Cold, dry air
700 mb
10,000 ft

L
Warm, moist air
Low-level jet
850 mb
5000 ft

H
Cold, dry air
L
Tornadoes
Warm, humid air
Surface

© 1998 Wadsworth Publishing Company/ITP

tropopause

cold air

strong wind

z(km)

dry air

stable layer   wind shear
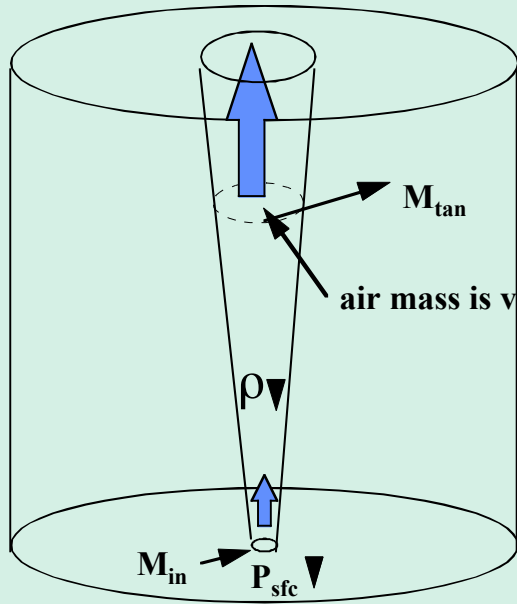
warm, moist air

Severe-thunderstorm environment

Dynamic condition for formation of the mesocyclones and supper cell:

Under strong wind share, a horizontal cyclonical vortex can rise following a spiral motion and form a mesocyclone.

z ↑   u →

very strong vertical shear of the horizontal wind

strong horizontal vortex

© 1998 Wadsworth Publishing Company/ITP

rapid stretch of the vortex accelerate the rotation

z ↑

u →

the horizontal vortex is bended by the vertical motion generated inside of convection

convection

A vortex tube is titled vertically to form a mesocyclone.

M_{tan}

air mass is vacuumed out of the vortex
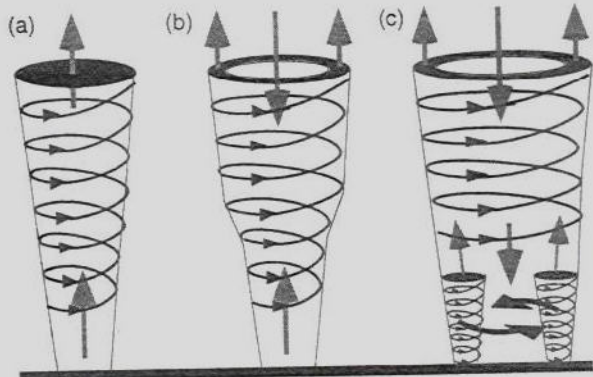
ρ ▼

M_{in} P_{sfc} ▼

for a larger swirl ratio

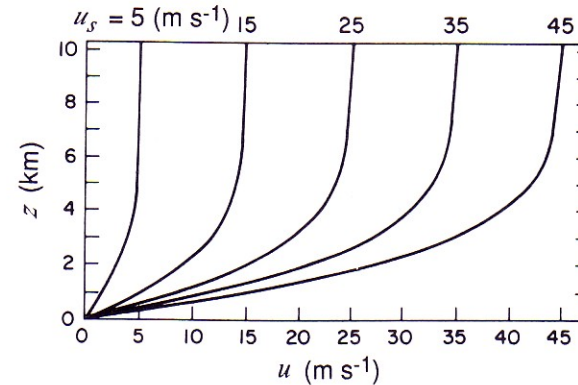

Figure 15.11
Tornadoes with swirl ratios (S) of: (a) S = 0.3 ; (b) S = 0.8 ; and
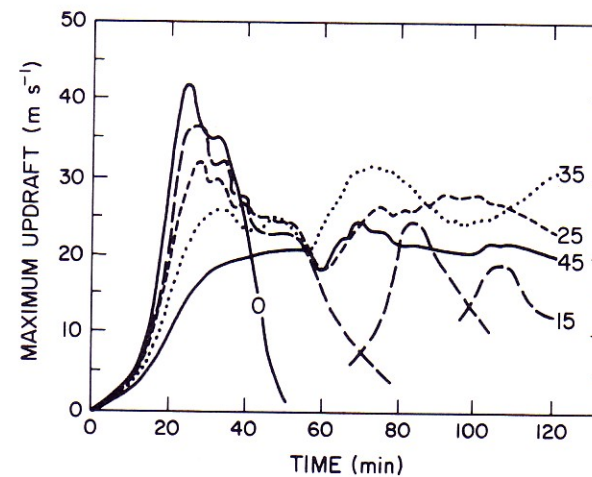(c) S = 2.0 .

- No shear: single, short lived cumulus cell

- weak shear: multi-cells

- Stronger shear: MCC

- Strongest shear: single supercell convection

What are the dynamic and cloud microphysical causes?

Figure 8.15 Profiles of wind speed u used in three-dimensional model simulations of multicell and supercell thunderstorms. Profiles becomes asymptotic to u_s. (From Weisman and Klemp, 1982. Reprinted with permission from the American Meteorological Society.)

Figure 8.16 Results of three-dimensional model simulations of thunderstorms under different amounts of wind shear. The quantity plotted is the maximum vertical velocity as a function of time for different values of the wind-shear parameter u_s (m s^{-1}), which is the number plotted next to each curve. (From Weisman and Klemp, 1982. Reprinted with permission from the American Meteorological Society.)

Clouds/precipitation formed by Mid-latitude frontal systems:
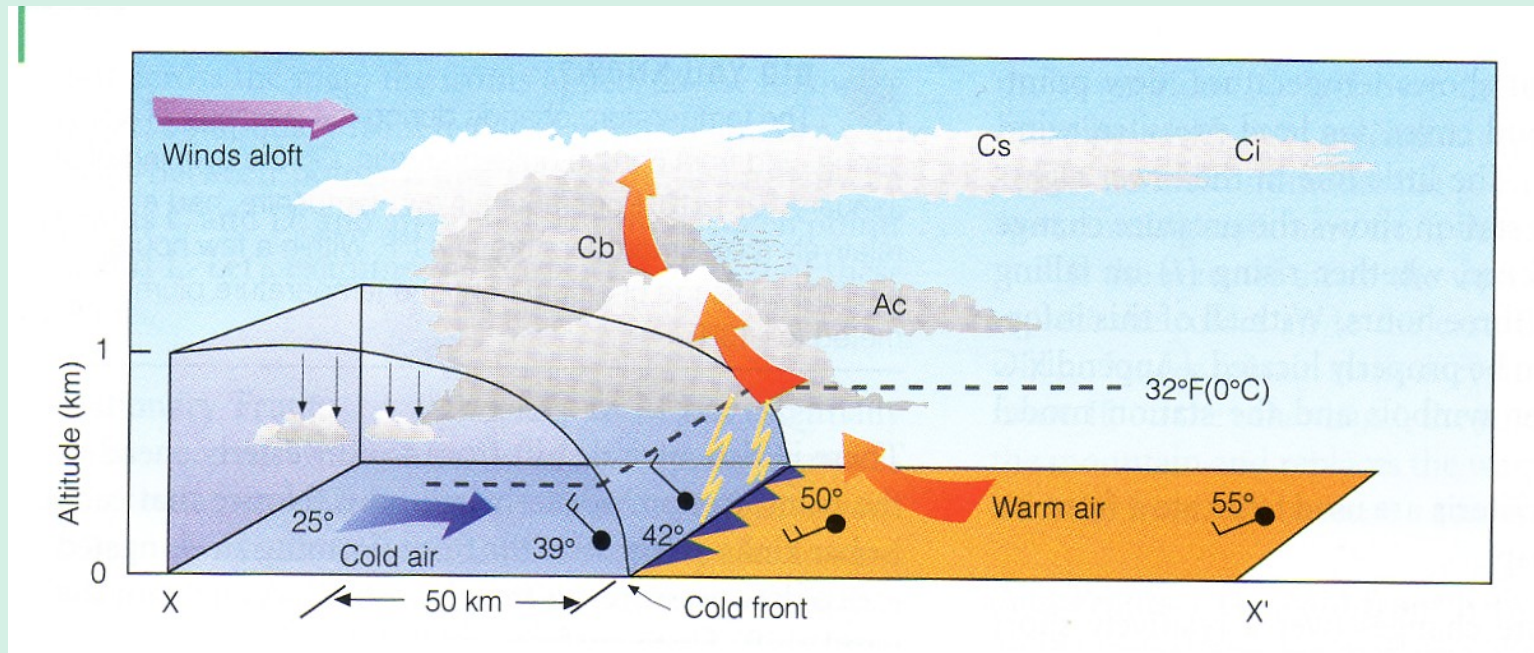
- *Cold fronts:*
- a zone where cold, dry stable polar air is replacing warm, moist and unstable subtropical air.
-
- Across a cold front from warm to cold side:
  - i. temperature drops rapidly
  - ii. wind speed increases and wind direction changes
  - iii. pressure decreases first and then increases
  - iv. clouds change from cirrus to nimbocumulus to stratus or stratocumulus
  - v. a narrow band of heavy precipitation associated with nimbocumulus.
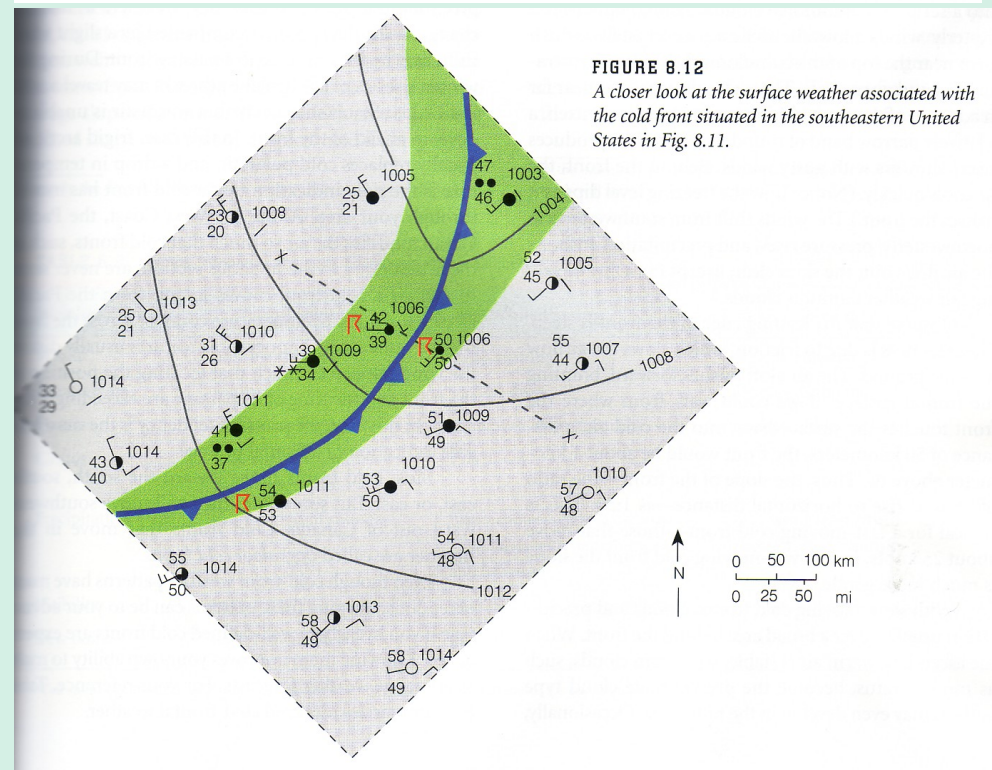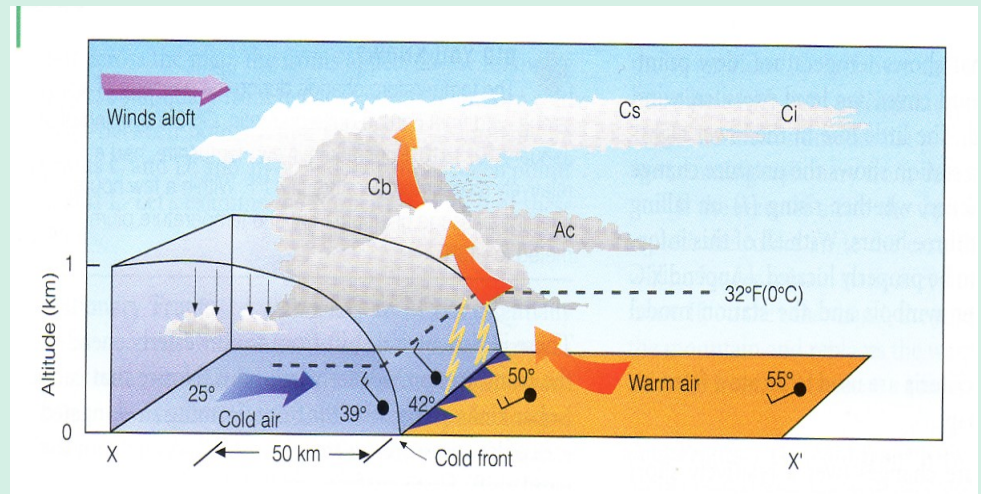
FIGURE 8.12
A closer look at the surface weather associated with the cold front situated in the southeastern United States in Fig. 8.11.
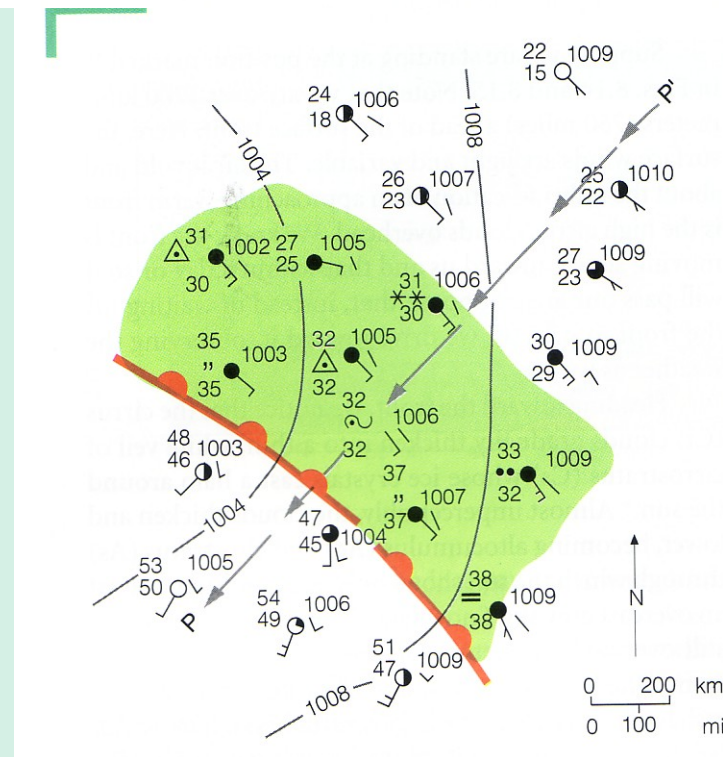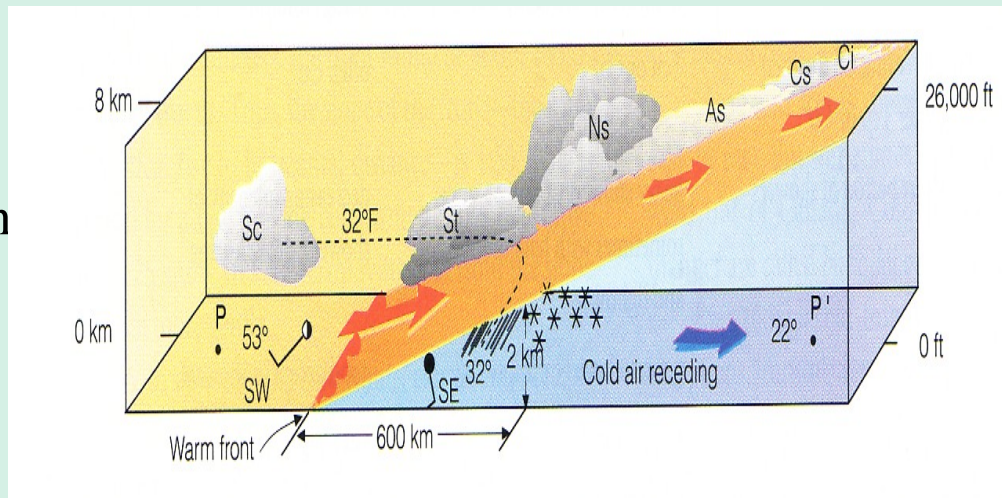
Warm fronts:

- Occurs when the advancing warm air replaces the retreating cold air.

Across a warm front from cold to warm side:

i. temperature rises and pressure decreases

ii. surface wind change direction

iii. clouds: Ci $\Rightarrow$ Ns $\Rightarrow$ St

iv. light-to-moderate rain or snow

v. temperature inversion $\Rightarrow$ no inversion

Sea Breeze and mountain valley breeze:
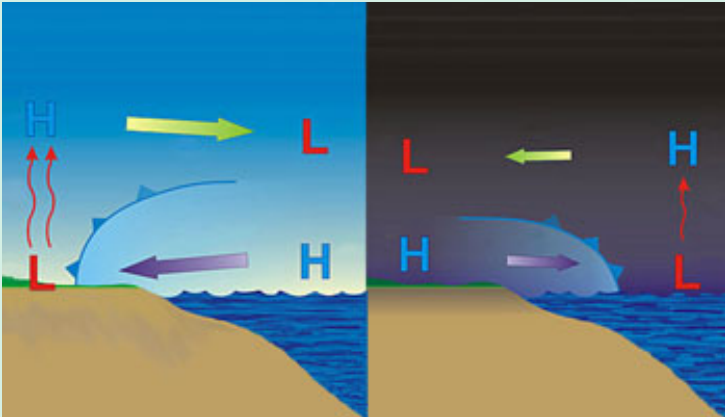
Surface heating gradient generates
Mesoscale circulation and dynamic
Lifting to form clouds/rainfall.
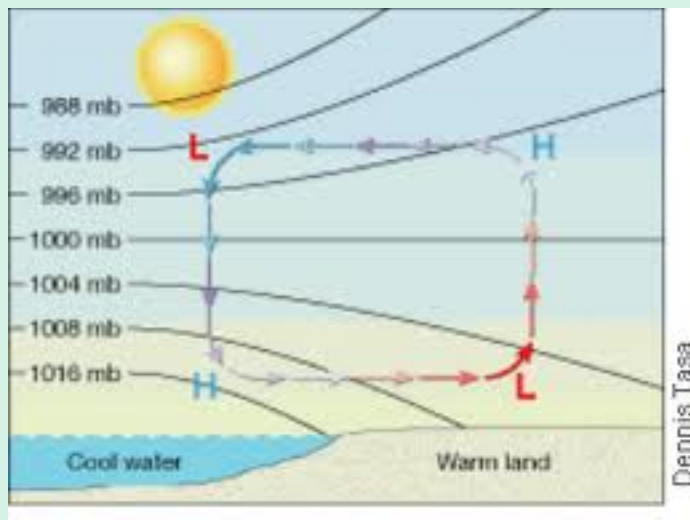
mountain valley breeze:

Cloud & rainfall form along mountain top in early afternoon,
In valley at night.
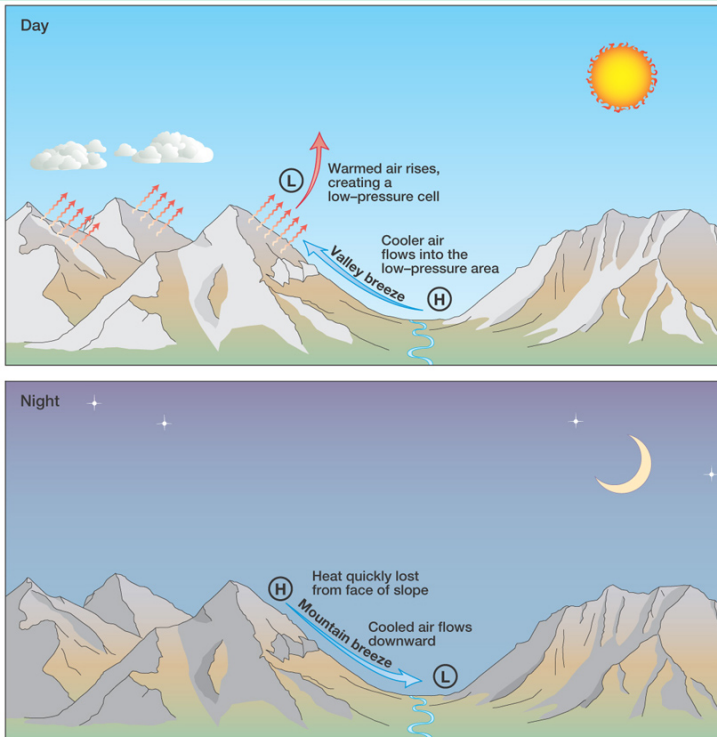
Cloud microphysical process in real clouds:

"seeder zone"
(~20% of rainfall)

Feeder zone (~80%
of rainfall)
Mainly deep
Stratiform cloud

Melting band (~0%)

Rain **region** (0%)
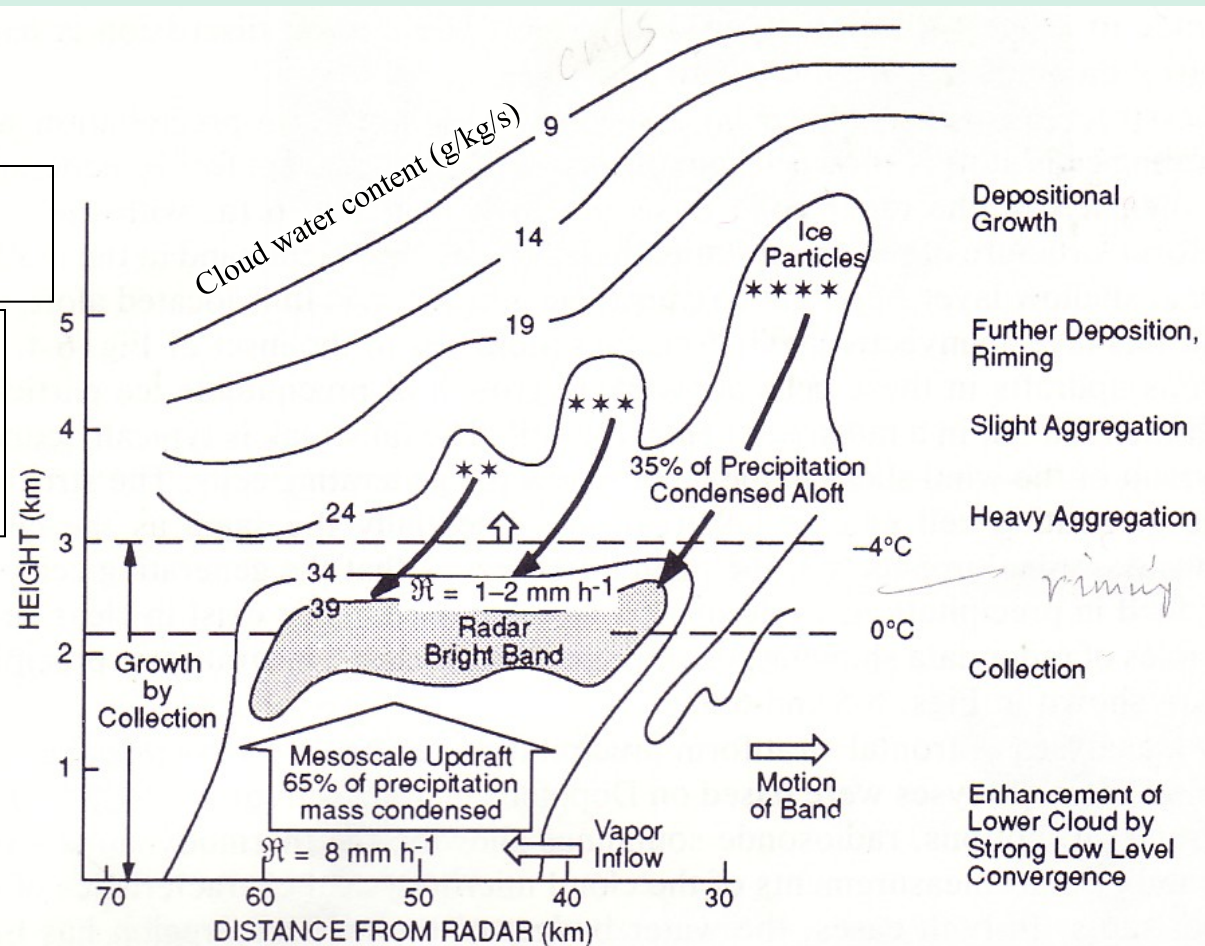
Figure 6.8 Schematic of the dynamical and microphysical processes in a stratiform frontal rainband over western Washington State. (From Houze *et al.*, 1981.)

Interaction between cloud microphysical processes:

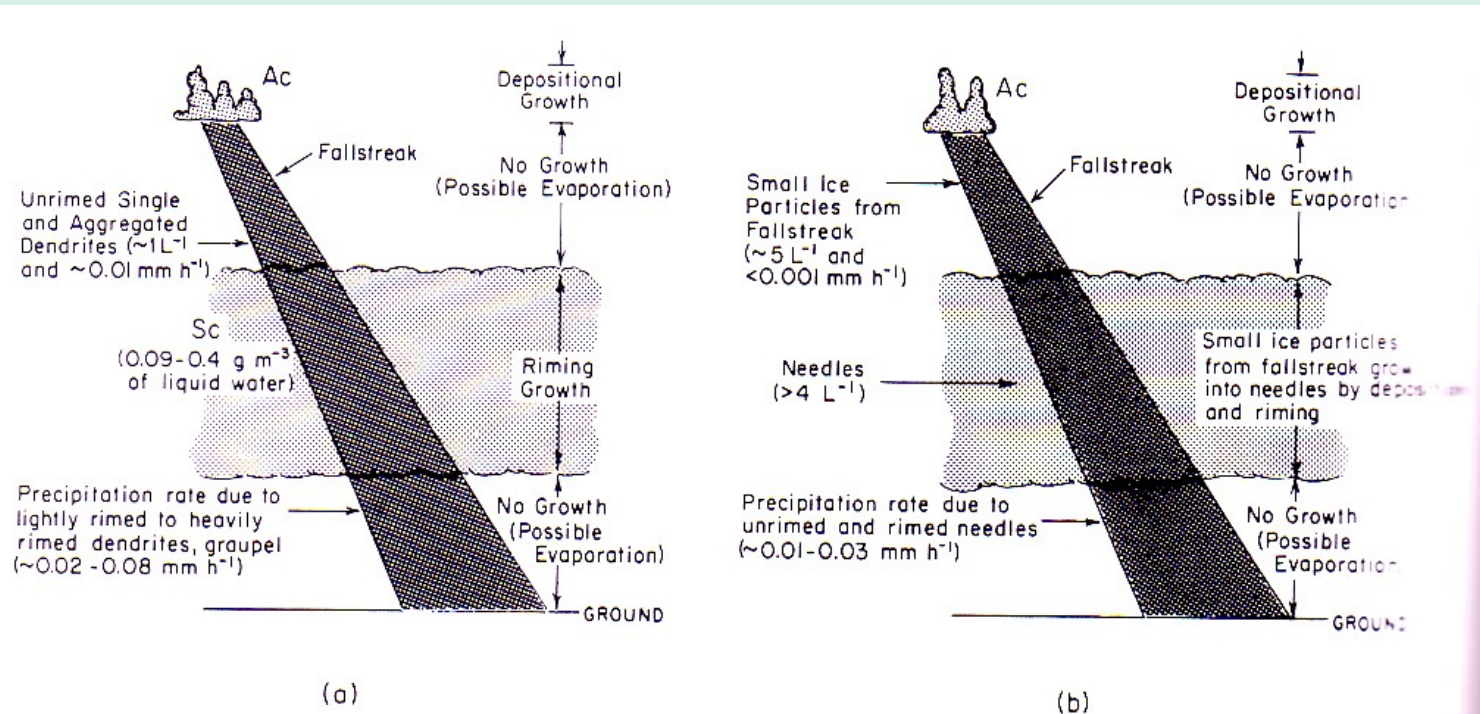**Figure 5.46** Schematic of interaction of altocumulus and stratocumulus clouds. (a) Dendritic crystals in a fallstreak from the altocumulus fall into the stratocumulus, where they grow by riming and reach the ground as light precipitation. (b) Small ice particles in a fallstreak from the altocumulus grow into needles in the stratocumulus and contribute to the precipitation at the ground. (From Locatelli et al., 1983. Reproduced with permission from the American Meteorological Society.)

Ice crystals fall from altocumulus grow by riming in stratocumulus below and produce precipitation. A_c and S_c alone would not produce precipitation.

Interaction between cloud microphysics and dynamics:

Direction of convection movement

Major ice enhancement

Further ice enhancement

ANVIL ICE

TURRET (1 - 3 km)

ICE STRANDS

Maximum concentration of ice particles

VIRGA

TUFTS (100 - 200 m)

AGGREGATION ZONE

0°C

0°C

COLLAPSE OF UPDRAFT

PRECIPITATION

Strong updraft

Strong updraft

Strong updraft

UPDRAFTS

PRECIPITATION TRAILS
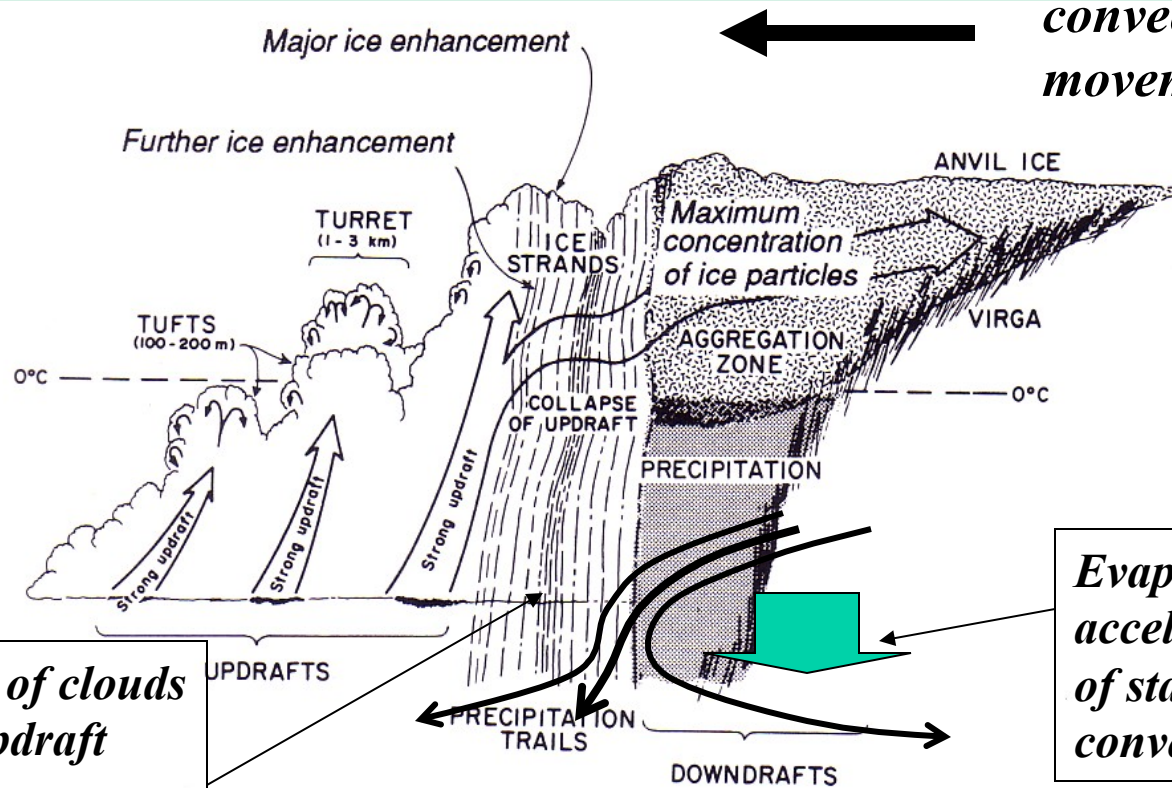
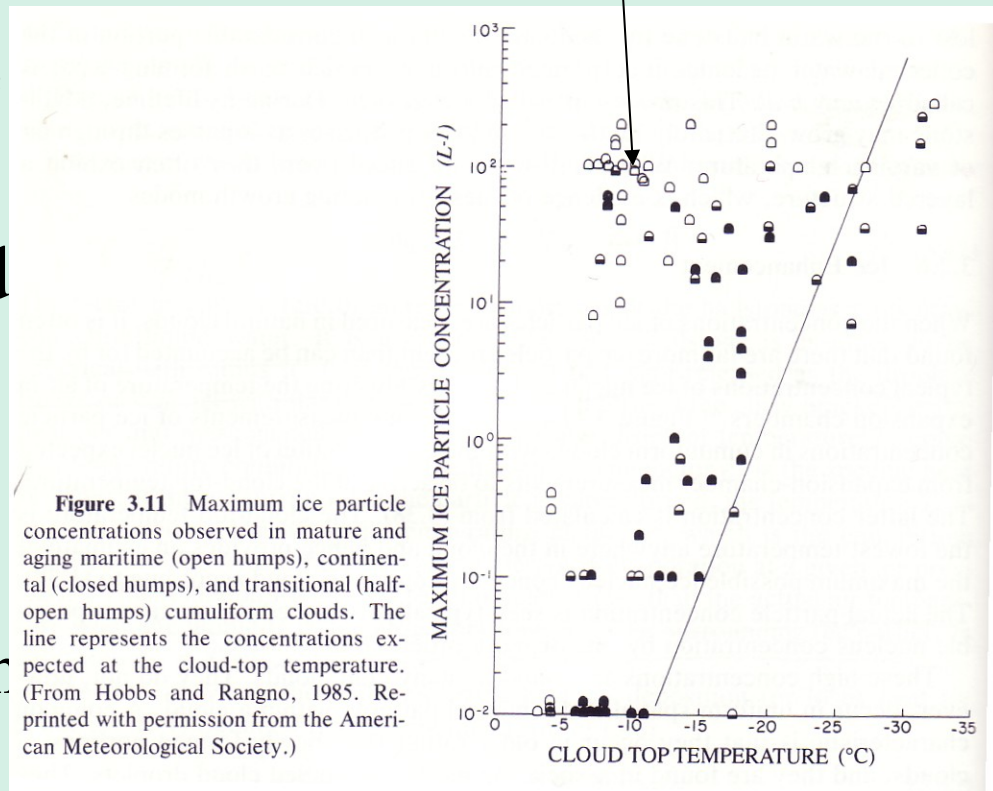DOWNDRAFTS

Downdrafts of clouds drops kill updraft

Evaporative cooling accelerate downdraft of stable air, putting convection forward

Figure 8.1 Empirical model of a small cumulonimbus cloud. Based on about 90 research aircraft penetrations of small cumulonimbus and large cumulus clouds. (From Hobbs and Rangno, 1985. Reprinted with permission from the American Meteorological Society.)

Ice enhancement

Possible causes:

- Fragmentation of ice crystals
- Ice splinter produced in riming
- Contact nucleation
- Condensation or deposition uncleation

Figure 3.11 Maximum ice particle concentrations observed in mature and aging maritime (open humps), continental (closed humps), and transitional (half-open humps) cumuliform clouds. The line represents the concentrations expected at the cloud-top temperature. (From Hobbs and Rangno, 1985. Reprinted with permission from the American Meteorological Society.)

Cloud droplets being rapidly lifted to anvils and detrained out of convection

Repeat circulation in convection forms graupels and hails.

Figure 8.12 (a) Vertical cross section of cloud and radar echo structure of a supercell thunderstorm in northeastern Colorado. The section is oriented along the direction of travel of the storm, through the center of the main updraft. Two levels of radar reflectivity are represented by different densities of hatched shading. The locations of four instrumented aircraft are indicated by C-130, QA, DC-6, and B. Bold arrows denote wind vectors in the plane of the diagram as measured by two of the aircraft (scale is only half that of winds plotted on right side of diagram). Short thin arrows skirting the boundary of the vault represent a hailstone trajectory. The thin lines are streamlines of airflow relative to the storm. To the right is a profile of the wind component along the storm's direction of travel. (b) Vertical section coinciding with (a). Cloud and radar echo are the same as before. Trajectories 1, 2, and 3 represent three stages in the growth of large hailstones. The transition from stage 2 to stage 3 corresponds to the reentry of a hailstone embryo into the main updraft prior to a final up–down trajectory during which the hailstone may grow large, especially if it grows close to the boundary of the vault as in the case of the indicated trajectory 3. Other, less-favored hailstones will grow a little farther from the edge of the vault and will follow the dotted trajectory. Cloud particles growing within the updraft core are carried rapidly up and out into the anvil along trajectory 0 before they can attain precipitation size. (From Browning and Foote, 1976. Reprinted with permission from the Royal Meteorological Society.)

Lightning and cloud microphysics

- *Charge reversal temperature: -10C ~ -20C*
  - *Colder than this, negative charges are transferred to grauple*
  - *Warmer than it, positive charges are transferred to graupel.*
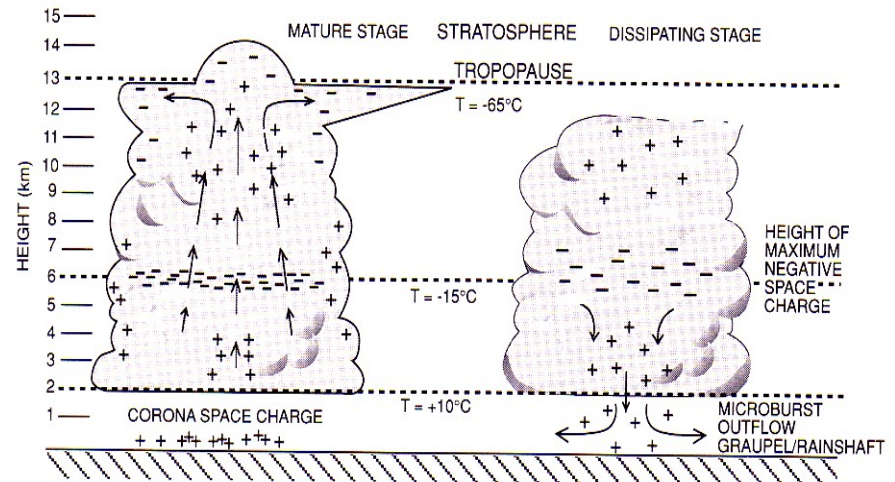
Figure 8.3 Schematic of the electrical structure of a cumulonimbus cloud. Positive and negative signs indicate the polarity of the charge at various locations. Streamlines indicate direction of airflow. (From Williams, 1988. © Scientific American, Inc. All rights reserved.)